Dynamic Contrast-Enhanced MRI Phenotyping of Pituitary Microadenomas and Macroadenomas: Integrated Correlation With Prolactin Profile and Clinical Presentation

Safa Musadaq Abd-AL Rahman

Department of the Radiologist Technology, Collage of Health and Medical Technology, AL-Zahraa University for Women, Karbala, Iraq; email: safa.musadaq@alzahraa.edu.iq

Abstract

Pituitary adenomas are common sellar lesions with heterogeneous radiological, hormonal, and clinical presentations. This study evaluated the role of dynamic contrast-enhanced MRI (DCE-MRI) in discriminating pituitary microadenomas from macroadenomas and correlating imaging findings with serum prolactin levels and clinical manifestations. A prospective cross-sectional study included 100 patients with suspected pituitary lesions who underwent conventional T1-weighted, T2-weighted, DCE-MRI, delayed post-contrast MRI, and serum prolactin assessment. MRI detected abnormalities in 75% of cases ($p<0.001$), including microadenomas in 44%, macroadenomas in 31%, and non-adenomatous findings in 25%. Microadenomas predominated in females, with mild prolactin elevation in 100%, irregular menstrual cycles in 58.9%, and mild galactorrhea in 58.9%. Macroadenomas were more common in males, with severe prolactin elevation in 72.2% and severe galactorrhea in 48.1%. Non-adenomatous cases showed normal prolactin and absence of galactorrhea in 100%. Pre-contrast T1-WI showed the highest signal score in non-adenomas (mean=3.0) and the lowest in macroadenomas (mean=1.0; $p<0.001$). DCE-MRI demonstrated heterogeneous enhancement as the most frequent pattern (31%), followed by hypo enhancement (22%) and homogeneous early enhancement (15%). Integrating DCE-MRI with prolactin profile and clinical presentation may improve characterization and diagnostic stratification of pituitary adenoma subtypes.

Keywords: Pituitary adenomas, Microadenoma, Macroadenomas, Dynamic contrast-enhanced MRI, Prolactin, Hyperprolactinemia.

1. Introduction

Pituitary adenomas are the most common intracranial tumors affecting 10-25% of the population, with prolactinomas being the most frequent functional type [1]. Recent cross-sectional studies have reported that the prevalence of symptomatic pituitary adenomas ranges from 7.76 per 10,000 to approximately 1 in every 1,064 individuals' rates that are 3 to 5 times higher than previously estimated [2,3]. While most Pituitary adenomas are histologically benign and rarely undergo malignant transformation, they often exhibit clinically aggressive behavior due to mass effect or hormone hypersecretion or deficiency [4]. The Pituitary gland is called "master gland" of the endocrine glands. The location of the gland is within the Sella turcica of the sphenoid bone or the hypophyseal fossa. Despite its small size, A variety of tumors can arise within it, its position deep within the skull base [5,6]. An essential part of the human body, the Pituitary gland, or hypophysis cerebri, carries out essential tasks for maintaining life [7].

Pituitary glands are produced by pituitary hormone are special chemical messengers. This pituitary gland regulates numerous bodily functions, including growth, maturation, reproduction, metabolism, stress response, circadian rhythm, and ageing. It also contains stem cells, which are essential for cell differentiation, turnover, and reactions to stress, disease, and physiological stimuli as well as hormone signaling. The hormones of the Pituitary gland are protein or polypeptide in nature and vary in complexity [8]. Prolactin is a protein hormone secreted by the acidophilic lactotroph cells of the anterior pituitary gland. Chemically, prolactin is like a growth hormone composed of 199 amino acids and forms after a 28-amino acid signal peptide is proteolytically cleaved from the prolactin prohormone (pre-prolactin) [9]. Hyperprolactinemia represents one of the most frequent pituitary disorders, manifesting gender-specific clinical symptoms. In women, it is commonly associated with irregular menstrual cycles, Galactorrhea, and hirsutism, whereas in men it often leads to erectile dysfunction and gynecomastia. Beyond these manifestations, hyperprolactinemia disrupts the gonadal axis, resulting in reduced libido and infertility in both sexes. Reported prevalence ranges from approximately 0.4% in the general adult population to 9–17% among women with reproductive disorders [10]. Microadenoma (MIA), this has a diameter <1 cm and often endocrinologically, MIA this depresses the floor of the Sella turcica expands on the side of the gland, causing a subtle upwardly convex bulge of the gland. While Macroadenomas (MA), this has a diameter > 1cm [11].

Magnetic Resonance Imaging (MRI) remains the gold standard for Pit tumor evaluation, offering superior soft tissue contrast and spatial resolution compared to Computed Tomography (CT), which allows clear visualization of the optic chasm, optic nerves, cavernous sinuses [12]. Conventional T1-weighted image (WI), and T2-WI sequences provide critical information on tissue characteristics, while dynamic contrast-enhanced MRI (DCE-MRI) improves the detection of small MIA, enables differentiation of tumor subtypes, and supports clinical decision-making [13, 14]. Despite its established role, few studies have systematically integrated MRI findings with clinical features and hormonal profiles in a single dataset.

The present study aims to evaluate the diagnostic performance of DCE-MRI in characterizing pituitary adenomas, with particular emphasis on its ability to differentiate MIA and MA in correlation with serum prolactin levels and clinical presentations. By integrating imaging, hormonal, and clinical features, this research seeks to enhance diagnostic accuracy and optimize management strategies for pituitary tumors.

2. Material and methods:

2.1. Patient selection criteria

Patients were enrolled based on predefined inclusion and exclusion criteria to ensure diagnostic accuracy and homogeneity of study sample

2.1.1. Inclusion criteria

Patients with suspected pituitary adenoma referred for MRI and hormonal testing. Patients aged 20 to 45 years who presented with clinical features suggestive of pituitary dysfunction, such as persistent headache, visual disturbance, menstrual irregularities, or Galactorrhea, were included. All enrolled patients underwent dynamic contrast-enhanced MRI of the pituitary gland and serum prolactin measurement within the same diagnostic session. Only patients with complete clinical, imaging, and laboratory records were considered eligible.

2.1.2. Exclusion criteria

Patients with a history of previous pituitary surgery, cranial radiotherapy, or those with contraindications to MRI or gadolinium-based contrast agents were excluded. Additional exclusion factors included pregnancy, known renal impairment, and incomplete imaging or hormonal data.

2.2. Sample Size Calculation and Power Analysis

A total of 100 patients, the final population was categorized into two groups: a control group $(n = 25)$, and pituitary adenoma group $(\mathrm{n} = 75)$, ensuring appropriate representation of both microadenoma (MIA) and macroadenomas (MA) patient data were anonymized, and the study was conducted in accordance with institutional ethical guidelines. Sample size estimation was performed using G*power software version 3.1.9.7. A priori power analysis was conducted by the parameters for an independent sample $\mathrm{t} - \mathrm{test}$, assuming a medium effect size $(\mathrm{Cohen's\ d} - 0.5)$, a significance $\alpha = 0.05$, and a power of 80% $(1 - \beta = 0.80)$, the group allocation ratio was set at 3:1 to reflect the expected prevalence abnormal to normal cases [15]. According to these parameters, the minimum required total sample size was calculated to be 64 participants, with 48 in the abnormal group and 16 in the control group. To enhance statistical validity, accumulation subgroup analyses (MIA vs. MA- Pituitary adenomas), and mitigate potential data loss due to missing values, the final sample size was increased to 100 patients. The effect size was estimated using the formula [16].

$$\mathrm{Cohen's\ d} = \left|\frac{\mu 1 - \mu 2}{\sigma}\right| \qquad (1)$$

Where: $\mu 1$ and $\mu 2$ represent the expected means of the two groups and σ represents the standard deviation.

2.3. Data Collection

The prospective cross-sectional study, at Marjan Medical City Hospital, Babylon, Iraq, from September 2024 to May 2026. The study population included 100 patients with clinical and radiological suspicion of Pituitary adenomas, referred to neuroimaging evaluation. All patients were referred from the Endocrinology and Neurology outpatient clinics to the Radiology Department for an MRI Unite examination of suspected pituitary disease. Following formal commencement and ethical approval. Following imaging, patients were sent to their respective specialist clinics for further clinical care. Demographic and clinical data were collected by structured face-to-face interviews with a standardized questionnaire and a pre-designed coding sheet. The data collected

were age, gender, weight, height, body mass index (BMI), WHO-based BMI classification, and pertinent clinical complaints such as Galactorrhea, headache, menstrual irregularities, and visual problems. Blood samples were collected during scheduled appointments, and serum prolactin levels were tested in the early morning before breakfast to ensure hormonal consistency.

3.3.1 Anthropometric Data

Body Mass Index (BMI) is a widely accepted anthropometric measure used to screen for macro-nutritional status, including undernutrition, normal weight, and overnutrition. BMI was calculated for all participants using formula [17]:

$$BMI = \frac{W}{H^2} \quad (2)$$

Where: W in kg represents to the weight of the body humans and (H) is the height of the body humans in meters.

According to the WHO, BMI is categorized as follows: underweight $(< 18.5\ kg/m^2)$, normal $(18.5 - 24.9\ kg/m^2)$, overweight $(25.0 - 29.9\ kg/m^2)$, and obese $(\geq 30.0\ kg/m^2)$. Obesity may be further subclassified into Class I $(30.0 - 34.9)$, Class II $(35.0 - 39.9)$, and Class III (≥ 40.0) based on severity [18].

2.4. Hormonal Stratification of Serum Prolactin Levels in Females and Males

Prolactin is a polypeptide hormone primarily released by the anterior pituitary gland that regulates lactation and other reproductive activities. Its secretion is principally regulated by hypothalamic dopamine, which has a tonic inhibiting effect. Several physiological factors influence prolactin levels, such as stress, pregnancy, and sleep [19]. Dysregulation of dopaminergic pathways is thought to be a major contributor to hyperprolactinemia. Serum prolactin levels are an important factor in diagnosing pituitary illnesses such as prolactinomas, pituitary microadenomas, and macroadenomas [20]. Given the physiological differences in prolactin concentrations between males and females, gender-specific reference ranges are essential to ensure diagnostic accuracy and proper classification of Hyperprolactinemia [21]. This study used stratified hormonal analysis to allow for more reliable associations between prolactin levels and pituitary disease.

2.4.1. Females-Prolactin Stratification

For females, the normal range was defined as $4.8 - 23.3\ ng/mL$. Prolactin levels were categorized into four levels; normal; $< 25ng/Ml$, mild elevation; $25 - 100ng/mL$, moderate elevation$100 - 250ng/mL$, and severe elevation $> 250ng/mL$, based on gender-specific thresholds [19, 22]. This classification facilitated improved interpretation of prolactin dynamics among female participants and enabled accurate stratification based on clinical-radiological correlations.

2.4.2. Males-Prolactin Stratification

In males, the physiological range for serum prolactin was considered lower than in females, typically between $4.0 - 15.2\ ng/mL$. Accordingly, male prolactin levels were categorized into; normal $< 20\ ng/mL$, mild elevation $20 - 80\ ng/mL$, moderate elevation $80 - 200\ ng/mL$, and severe elevation $> 200\ ng/mL$ [19]. This stratification was essential for identifying clinically significant hyperprolactinemia and its association with male pituitary adenomas and non-adenomatous lesions.

2.5. Clinical Variables Assessed

2.5.1. Menstrual Disturbance Classification in Female Patients

As part of the clinical data collection process, female patients were evaluated for menstrual irregularities, which represent a common clinical manifestation of pituitary adenomas, particularly those associated with hyperprolactinemia. [20]. Menstrual patterns were systematically classified into four clinically recognized categories; regular cycle (normal), irregular cycle (Oligomenorrhea), amenorrhea ≥ 3 months (secondary amenorrhea and never had menses (primary amenorrhea) [22, 23]. This classification was based on standard endocrinologically definitions and was recorded at the time of clinical presentation. The categorization was utilized to correlate the type of menstrual disturbance with tumor type (microadenoma, macroadenomas, or non-adenoma), prolactin level, and MRI findings.

2.5.2. Galactorrhea

Galactorrhea is defined as the inappropriate secretion of breast milk in individuals who are neither postpartum nor breastfeeding, and it is most associated with elevated serum prolactin levels [24]. This condition is strongly linked to pituitary tumors, particularly prolactin-secreting adenomas, and its severity often reflects the degree of hormonal disturbance [25]. In this study, Galactorrhea was classified into four categories; no Galactorrhea, mild (+), moderate (++), and sever (+++), providing a standardized clinical assessment tool for correlating prolactin levels and tumor characteristics [26]. This classification is widely used in clinical practice to evaluate symptoms severity and guide diagnostic interpretation [24,25,26].

2.5.3. Visual Symptoms

Visual disturbances were evaluated as part of the clinical assessment due to their strong association with pituitary adenomas, particularly in macroadenomas that extend to the suprasellar region and compress the optic chiasm. In this study, visual symptoms were classified into two categories; yes (presence of any visual disturbance) and no (absence of visual symptoms). The assessment was based on patient history and ophthalmological evaluation, including visual acuity and field testing when indicated [27, 28]. Documenting visual symptoms provides a crucial clinical marker for tumor size and extension, as numerous studies have demonstrated that visual field defects such as bitemporal hemianopia are among the earliest and most significant indicators of optic pathway involvement in pituitary adenomas [24, 26].

2.5.4. Headache

Headache is a common presenting symptom in patients with pituitary adenomas and is often reported as an early clinical manifestation before hormonal or visual disturbances develop. Its pathogenesis is mainly attributed to local mass compression effect on optic Chiasm, and in some mass's foe central and suprasellar [29]. Clinical variables were extracted from patient records and coded for statistical analysis, headache was recorded as a binary variable; yes = 1, no = 2. Clinical studies have demonstrated that the severity of headache correlates more strongly with tumor expansion rather than hormonal activity, and macroadenomas are frequently associated with persistent headache compared to microadenomas [30]. In this study, headache was assessed as a binary variable and categorized into yes (presence of headache) or no (absence of headache) during initial clinical evaluation [28].

2.5. MRI Technical Considerations

2.5.1. Principle of MRI

The basic principles of MRI depend on the fact that the nuclei of certain elements align with the magnetic force when depend in a strong magnetic field. At the field strengths currently used in medical imaging, hydrogen nuclei (protons) in water molecules and lipids are responsible for at the resonant frequency of hydrogen is applied, a proportion of the protons change alignment, flipping through a present angle, and rotate in phase with one another [31]. MRI is a non-invasive diagnostic modality that utilizes strong magnetic fields and radiofrequency (RF) pulses to generate high-resolution images based on proton relaxation properties within tissues [32]. Following the radiofrequency pulse, the protons return (realign) to their original positions. As the protons realign (relax), they induce a signal which, although very weak, can be detected and localized by copper coils placed around the patient [31]. An image representing the distribution of hydrogen protons can be built up [31]. The various types of signals obtained are labeled as T1, T2 relaxation signals, the magnetic resonance signals have specific tissue characteristics. These are analyzed by a computer and reconstructed mathematically by a process known as " Fourier transformation" into sectional images of the human body, T1- WI, Proton density, and T2-WI [33].This technique provides superior soft tissue contrast, making it the gold standard for pituitary gland evaluation due to its ability to differentiate normal gland tissue from adenomas and assess adjacent neurovascular structures [34].

2.5.2. MRI Protocols

MRI protocol refers to a predefined set of imaging parameters and sequences selected to optimize image quality for a specific anatomical region or clinical indication [32]. All imaging was performed using a Philips 1.5 Tesla MRI closed system (Philips Medical System, Best, The Netherlands) equipped with a dedicated head coil.

2.5.2.1. MRI Parameters (Acquisition Settings)

There are many factors available to the technologist when setting up a sequence. The appropriate selection of the parameters determines the weighting, improved quality of images and sensitivity to pathology. Flip angle. Repetition Time (TR). Echo Time (TE). Slice thickness, to give slice a thickness, a band nucleus must be excited

by the excitation pulse. Increase of slice thickness, increase SNR, coverage of anatomy and partial volume whereas spatial resolution is decrease [33]. Spacing is the gap between two slices. When acquiring a multiplanar, single acquisition, spacing controls crosstalk. As spacing increases, crosstalk decreases [33]. Matrix Size. Field of view, more commonly known by the abbreviation FOV. This is the area being imaged and may be symmetrical or rectangular the FOV is related to the amplitude of the phase (G_P) and frequency (G_F) gradients as follows;

$$\gamma\, G_F = BW/FOV \quad (3)$$

$$\gamma G_P\, t_P = 0.5\, N_P/FOV \quad (4)$$

Where BW, $N_P$and t_P are the receiver bandwidth, phase encoding matrix and the duration of the phase encoding gradient respectively [21]. Small FOV produces high resolution, low Signal to noise ratio (SNR), and increases the minimum TE value = SAT pulses decrease the number of slices in an acquisition [33]. Flip angle, the resulting orientation, α degrees of the net magnetization with respect to the B_0 field, following the application of an RF excitation pulse [35]. It is given by formula

$$\alpha = \gamma B_1\, t \quad (5)$$

Where B_1 and t is the strength and duration of the RF pulse respectively, and γ is the gyromagnetic ratio.

Repetition Time (TR) controls the amount of longitudinal magnetization (LM) that recovers before the next RF excitation pulse is applied. A long TR allows full recovery of LM so that more is available to be flipped into the transverse plane in the next TR. Echo Time (TE), the amount of cohort transverse magnetization (TM) that decays before an echo is collected. A long TE allows considerable decay of cohort TM before the echo is collected, while a short TE does not. Matrix Size refers to the number of pixels in the frequency-encoding and phase-encoding directions of an MR image. It determines the spatial resolution by defining how many discrete samples are collected along each axis of the [36].

2.5.2.2. MRI Sequences and Dynamic Contrast Studies

A. Dynamic Contrast-Enhanced MRI (DCE-MRI) Protocol and Rationale in This Study

In this study, the dynamic contrast-enhanced MRI technique was utilized to evaluate pituitary gland lesions by assessing enhancement signal patterns rather than performing pharmacokinetic or time–intensity curve (TIC) analysis. Dynamic, the repeated acquisition of images at the same slice location [35]. The primary aim was to categorize enhancement into clinically relevant qualitative patterns, which is considered a reliable and widely accepted approach in pituitary imaging when early enhancement behavior is the diagnostic focus. Dynamic imaging was performed immediately after intravenous injection of gadolinium-based contrast material using an automated power injector to ensure standardized delivery. Sequential T1-WI (DCE-MRI) images were acquired rapidly in the coronal section to capture early arterial and venous phases within the first 90 seconds after injection. The enhancement patterns were visually assessed and classified into predefined categories: (Hypo enhancing, early heterogeneous enhancement, homogeneous early enhancement, small, delayed enhancement, focal delayed enhancement, normal physiological enhancement). Enhancement, an increase in signal intensity (usually) caused by the administration of contrast agents. It may also refer to increasing the signal of low sensitivity nuclei by the process of hyperpolarization [35]. The decision not to perform TIC analysis or calculate pharmacokinetic parameters (such as Ktrans or Kep) was based on the study objective, which focused on correlating enhancement signal patterns with body mass index (BMI) classifications and clinical variables (e.g., Galactorrhea, prolactin level). Qualitative pattern analysis provides practical diagnostic value in routine clinical practice and remains the standard in many institutions for pituitary imaging [31].

B. Contrast Agents (Gd-DTPA)

A substance an "exogenous chemical agent", which is used to alter the signal properties within the image. Most contrast agents usually shorten relaxation times, but spin-density agents also exist. The paramagnetic types cause a T1 shortening enhancement effect. The most common paramagnetic agents are the extracellular gadolinium-based agents. It consists of a gadolinium ion chelated to three diethylenetriamine pentaacetic acid (DTPA) producing a linear ionic complex with a -2 charge. This is chemically balanced with two meglumine charges. The resulting agent is called dimeglumine gadopentetate and is marketed commercially as Magnevist [35]. These agents improve lesion detection and characterization by highlighting abnormal vascularity. A gadolinium-based contrast agent single dose, (0.1 mmol/kg body weight) was injected at a rate of 2 mL/s, followed by a 10 mL

saline flush to ensure complete bolus administration. Dynamic images were acquired immediately after injection at 10–12-second intervals for 60–90 seconds to capture the early enhancement kinetics of the pituitary gland.

C. Conventional Sequences pre-contrast for the Pituitary Gland

They are essential for structural imaging and include T1-WI-Spin Echo (SE), sagittal and coronal thin slice section, T2-WI-Turbo Spine Echo (TSE), sagittal and coronal thin slice section. TSE, and SE sequences are commonly used to reduce scan times while preserving image quality [36]. These sequences provide excellent soft-tissue contrast, enabling accurate visualization of pituitary anatomy and pathology [37]. In this study, used T2-WI-axial section or T2-FLAIR-axial section of the brain to demonstrate all the brain tissues pathological and anatomical.

D. Additional Delay post-contrast imaging Protocol for the Pituitary Gland

Following the initial dynamic contrast-enhanced T1-weighted acquisition, delayed imaging was performed to improve the detection of subtle or slow-enhancing pituitary lesions. Delayed sagittal and coronal T1-WI-SE sequences were obtained 3 to 5 minutes after contrast injection, using identical plane orientation and imaging parameters as the baseline pre-contrast scans. This delay interval aids in differentiating true pathological enhancement from physiological pituitary tissue, especially helpful in identifying microadenomas that display delayed uptake. Enhancement patterns were visually classified into three categories: (small, delayed enhancement, focal delayed enhancement, normal physiological enhancement). These patterns were determined qualitatively, based on the distribution and degree of signal relative to the surrounding gland tissue [38].

2.5.3. Patient positioning and Equipment for Examination

All patients were positioned supine on the MRI table with the headfirst into the scanner bore, using a dedicated head coil to ensure optimal signal-to–noise ratio and image quality. The head was aligned in the mid-sagittal plane, and foam pads were applied to minimize motion artifacts. Clear instructions were given to patients to remain still and avoid swallowing during acquisition [39]. For dynamic contrast-enhanced study, an automatic power injector (Medrad Spectris, Bayer Healthcare) was used for standardized contrast delivery [40].

2.5.4. Imaging planes

In this study, imaging of the brain used T2-WI-axial section or T2-FLAIR-axial section. Accurate planning of imaging planes is essential for optimal visualization of the pituitary gland and surrounding structures. In this study, two primary imaging planes were used: sagittal and coronal. Sagittal planning was performed based on axial reference images, with slice alignment parallel to the falx cerebri in both sagittal and coronal directions. The coverage extended from the floor of the sphenoid sinus to the genus of the corpus callosum (superior to inferior), laterally to include both cavernous sinuses, and anteroposterior from the ventral aspect of the pons to the anterior clinoid process. This plane allowed for optimal assessment of: (elevation or displacement of the optic chasm by Sellar or suprasellar masses, Invasion of the lesion into the sphenoid sinus, carotid siphon, or brainstem, Visualization of the pituitary stalk (infundibulum) and posterior pituitary, Bony changes of the Sella turcica, including expansion or erosion) [41]. Two controls determine tissue contrast TR (repetition time), and TE (time echo) of the scan. Spacing or inter-slice gap is the small space between two adjacent slices and can be measured by millimeters. It provides method to compensate for imperfect RF excitation pulse. Inter-slice gap allows the technologist to control the size of the imaging volume by increasing and decreasing space in between slices. There is a close relationship between the field of view (FOV) and the signal-to-noise ratio (SNR). When the matrix size is kept constant, the FOV determines the pixel size. Pixel size in the frequency-encoding direction is calculated by dividing the FOV in millimeters by the number of points in the frequency-encoding direction, while in the phase-encoding direction it is obtained by dividing the FOV by the number of points in the phase-encoding direction. Another limiting factor is the scan time, which increases directly with matrix size and represents a key determinant of the economic efficiency of MRI systems. Scan time can be calculated using the following equation: Scan time = TR × number of phase-encoding steps × number of signal averages (NSA) [echo train length (ETL)] [42]. Spin-Echo (SE), a classic sequence where a 90° pulse is followed by a 180° refocusing pulse to produce a clean echo. When timed for T_1 recovery, it generates a T_1-weighted image (WI). Regarded as foundational for generating accurate tissue contrast based on T_1 relaxation. Turbo (Fast) Spin-Echo (TSE/FSE), an advanced variation of spin-Echo where multiple 180° pulses generate a train of echoes. Each echo fills a different line of k-space within a single TR, significantly shortening scan time. When configured with a longer effective TE, the sequence emphasizes T_2 contrast image thus yielding T_2-WI-TSE [36].

Table (1): Practical Protocol for the Pituitary Gland

Study part	Sequence	Slice orientation	TR (ms)	TE (ms)	FOV (mm)	Slice Thickness (mm)	Gap (mm)	Matrix size
Brain Screening	T_2-WI-TSE T_2-FLAIR	Axial Axial	6816 9000	110 120	230*230 230*230	5 5	0.5 0.5	256*256 256*256
Pituitary Protocol	T_1-WI-SE T_1-WI-SE T_2-WI-TSE T_2-WI-TSE	Sagittal Coronal Sagittal Coronal	550 550 3000 3000	15 15 120 120	23*20.7 23*20.7 23*20.7 23*20.7	3 3 3 3	0.1 0.1 0.1 0.1	256*256 256*256 256*256 256*256
Dynamic Study	T_1-WI-=Dynamic during injection Gd	Coronal	4.3	1.8	230*230	2.5	0	256*256
Delayed post-contrast	T_1-WI-SE (3min Post Gd) T_1-WI-SE (5 min Post Gd)	Sagittal Coronal	550 550	15 15	23*20.7 23*20.7	3 3	0.1 0.1	256*256 256*256

2.6. Statistical Analysis

2.6.1. Software Description (Statistical Package for the Social Science SPSS)

SPSS is a comprehensive software package designed for statistical analysis in social science, healthcare, and research fields. It provides tools for data management, descriptive statistics, inferential analysis, hypothesis testing, regression modeling, and advanced analytics. SPSS also offers options for creating tables, and charts. The software interface includes features such as data view and variable view. Continuous variables were presented as mean ±standard deviation, while categorical variables were expressed as frequencies and percentages [43].

2.6.2. Hypothesis Testing and Significance Level (α)

A two-tailed hypothesis test was applied with a significance level of α = 0.05. The null hypothesis (H_0) assumed no significant difference between the compared groups, while the alternative hypothesis (H_1) indicated a significant difference. Fig (1) illustrates the standard normal distribution with rejection regions at $\pm Z(\frac{\alpha}{2})$, which defines the critical cutoff points for statistical decision making [44].

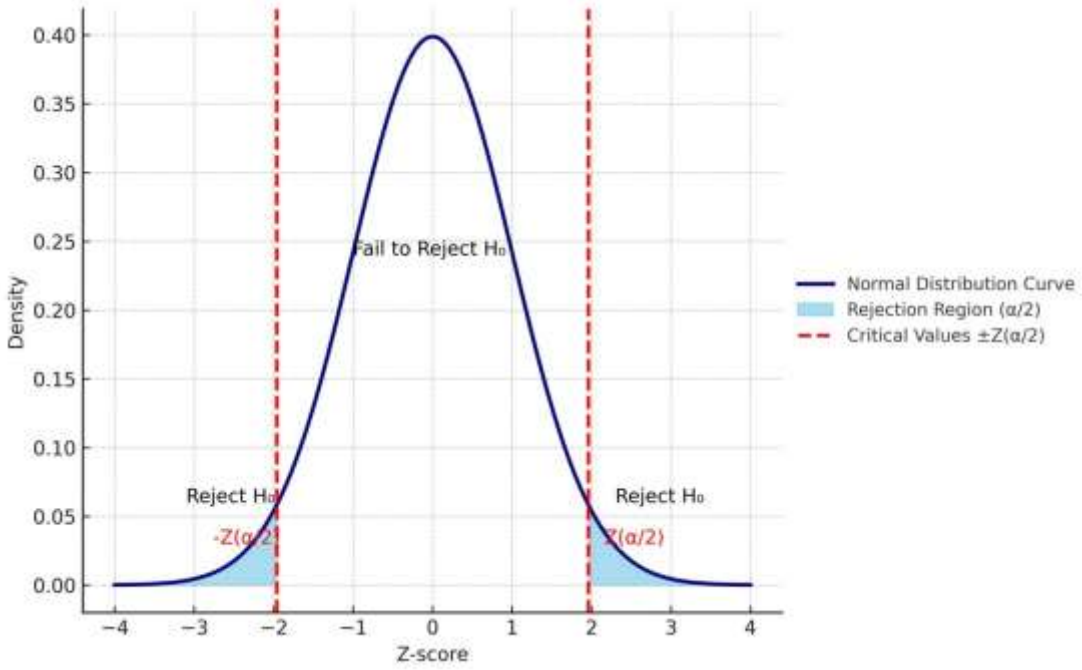

Fig (1): Standard Normal Distribution Illustrating Rejections at Significance Level α = 0.05 for two-tailed hypothesis testing

2.6.3. P-value

The P-value is a fundamental concept in statistical hypothesis testing that reflects the strength of evidence against the null hypothesis (H_0). It represents the probability of obtaining test statistics at least as extreme as the observed value, assuming the (H_0). is true. A small P-value (typically < 0.05) suggests that the observed data are unlikely under the (H_0), leading to its rejection in favor of the alternative hypothesis. Interpretation Criteria. (P≤ 0.05) Reject H_0 statistically significant result, while (P > 0.05) fail to reject H_0 not statistically significant. Mathematical representation for two, one -tailed tests respectively [44].

$$P - value = 2 \times P\ (Z \geq |Z\ Observed\ |) \quad (6)$$

$$P - value = P\ (Z \geq |Z\ Observed\ |) \quad (7)$$

Where; Z is the test statistic assuming the null hypothesis, $Z\ Observed$ is the calculated statics from the sample.

However, the P-value does not indicate the magnitude or clinical relevance of an effect; it only determines whether the result is statistically significant. Its interpretation should account for study design, sample size, and potential biases. Very small P-values may arise from trivial differences in large samples, while meaningful effects may fail to reach statistical significance in small samples. Therefore, P-values should be interpreted alongside confidence intervals, effect sizes, and subject-matter expertise. Importantly, statistical significance does not imply clinical or practical importance, emphasizing the need for a holistic evaluation of the findings [45].

$$P = P(\chi^2 \geq \chi_{observed})\ From\ chi - square\ distribution\ with\ df \quad (8)$$

2.6.4. Statistical Analysis of Diagnostic Performance Metrics

The diagnostic performance of MRI for the detection of pituitary adenomas was assessed by calculating sensitivity, specificity, and overall accuracy using standard formulas. The definitions of diagnostic accuracy measures, including sensitivity refer to the ability of a test to correctly identify patients with the disease (true positive TP), whereas specificity indicates the ability to correctly identify those without the disease (true negative TN). Accuracy reflects the overall proportion of correctly classified cases (both true positives and true negatives) among the total examined [46]. All calculations were based on a 2 × 2 contingency table (confusion matrix) comparing MRI findings with the reference standard (serum prolactin level) [47, 48].

$$Sensitivity = \frac{True\ Positive\ (TP)}{True\ Positive\ (TP) + False\ Negatives\ (FN)} \times 100$$

$$Specificity\ (\%) = \frac{True\ Negatives\ (TN)}{True\ Negatives\ (TN) + False\ Positives\ (FP)} \times 100$$

$$Accuracy\ (\%) = \frac{True\ Positives\ (TP) + True\ Negatives\ (TN)}{TP + TN + FP + FN} \times 100$$

Where TP refers to cases correctly identified as abnormal by MRI, TN refers to correctly identified normal cases, FP represents false positives, and FN represents false negatives. All statistical computations were performed manually and validated using SPSS software [46]. Results were expressed as percentages.

Table (2): Demographic Characteristic of the Study Population by Gender (Age & Weight Distribution, n=100)

Gender	mean ± Std. Deviation		Number of cases
	Age means (years)	Weight (Kg)	
Male	39.3 ± 5.69	79.03 ± 10.04	27
Female	30.16 ± 6.09	72.52 ± 10.99	73
Total mean	32.64±7.22	74.28±11.08	100
Overall Cases%	100.0%		

Table 2 presents, the demographic distribution of the study population (n = 100) categorized by gender, including age and weight. Most of the participants were female (73%), while male participants accounted for 27% of the total cases. The mean age of males (39.3 ± 5.69 years) was notably higher than that of females (30.16 ± 6.09 years), which may reflect differences in referral patterns or hormonal-related disease prevalence [49, 50]. The average weight was also slightly higher among males (79.03 ± 10.04 kg) compared to females (72.52 ± 10.99 kg), aligning with expected gender-based physiological differences. [51].

Table (3): Anthropometric Analysis of BMI Categories According to WHO Standards: Correlation with Mean Height and Distribution in a Clinical Population (n=100).

Classification BMI according to WHO	mean ± Std. Deviation		Number of cases
	Height mean (m)	BMI (kg/m^2)	
Normal	1.67 ± 0.062	22.56 ±0.86	36
Overweight	1.69 ± 0.069	27.54 ±1.88	44
Obesity classification I	1.67 ± 0.036	31.15 ± 0.90	13
Obesity classification II	1.55 ± 0.014	35.01 ± 0.64	7
Total	1.67 ± 0.06	26.74 ± 3.99	100
Overall Cases%			100%

Table 3 classifies the population according to WHO BMI standards, correlating with mean height and BMI values. The highest proportion of cases fell under the overweight category (44%), followed by normal BMI (36%), while obesity classes I and II represented 13% and 7%, respectively. This distribution indicates a predominance of increased body mass within the study group, which is important to consider when analyzing hormonal or pituitary-related pathologies. Previous research has shown that obesity is associated with altered pituitary function and increased prolactin levels, potentially due to changes in dopaminergic tone and adipose tissue hormone interactions [18, 52].

Table 4 The results show that most cases (75%) were classified as having abnormal MRI findings, with a significantly lower mean diagnostic score (1.42 ± 0.52). In contrast, only 25% of cases were classified as normal, exhibiting a higher mean score (2.96 ± 0.20). The statistical significance ($p < 0.001$) indicates a strong association between abnormal imaging results and adenomatous pituitary pathology. These findings support the diagnostic value of MRI in detecting subtle anatomical alterations in the pituitary gland, particularly in patients with suspected adenomas [31, 53, 54, 55].

Table (4): Comparison of MRI-Based Diagnostic Scores of the Pituitary Gland Between Normal and Abnormal Cases by One-way ANOVA.

Tumor Type	MRI Diagnostic Category	Mean ± Std. Deviation	Number of cases	P-value
Non-adenomas	Normal MRI	2.96 ± 0.20	25	

Adenomas (Microadenoma & Macroadenomas)	Abnormal MRI	1.42 ± 0.52	75	< 0.001**
Total		1.81± 0.81	100	
Overall Cases%			100%	

Fig 2 In this study, the MRI-based classification revealed that 75% of the cases exhibited abnormal pituitary findings, with a calculated mean = 1.75 ± 0.43. The remaining 25% were categorized as normal (mean = 1.25 ± 0.43). Statistical analysis showed a significant difference between the groups with a p-value < 0.001, indicating a strong association between abnormal imaging findings and suspected pituitary pathology**.** These findings highlight the sensitivity of MRI in detecting subtle structural abnormalities of the pituitary gland, including Pituitary adenomas [55, 56].

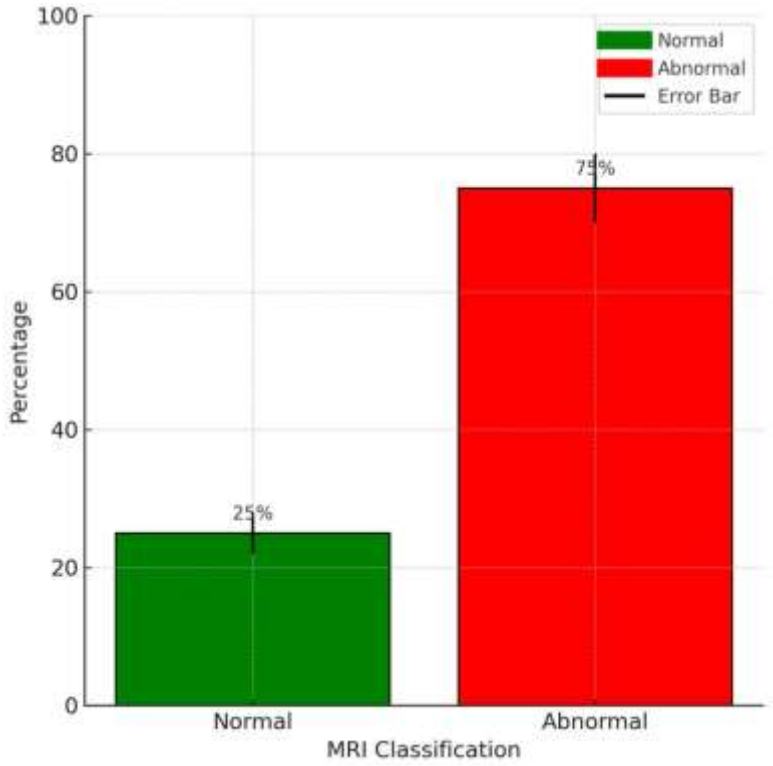

Fig (2): Distribution of Pituitary MRI Findings Showing Normal and Abnormal Classifications Among Patients.
Table 5 The MRI-based classification revealed that pituitary adenomas constituted most cases, with MIA at 44%nd MA at 31%, while non-adenomatous lesions accounted for only 25%. The significant p-value (p < 0.001) underscores the predominance of adenomatous tumors in the studied population. This distribution reflects global epidemiological trends, where Pituitary adenomas are the most frequently encountered pituitary lesions on imaging [19, 57].

Table (5): Proportional Distribution of Pituitary Tumor Subtypes Identified on MRI in the Study Population

Types of Tumors	Frequency	Percent	Cumulative Percent	P-value
Microadenoma	44	44.0%	44.0%	<0.001**
Macroadenomas	31	31.0%	75.0%	
Non-adenomas	25	25.0%	100%	
Total	100	100%		

Table 6 The highest mean gender code was observed in microadenomas (1.98 ± 0.151), indicating a predominant female prevalence approximately (95.5%). In contrast, MA had a significantly lower mean (1.42 ± 0.502), reflecting a higher male representation approximately (58%). The p-value (< 0.001) denotes a

statistically significant gender-based variation across tumor subtypes. These findings are consistent with existing literature indicating that microadenomas, particularly prolactinomas, are more frequently diagnosed in females, whereas macroadenomas have a higher prevalence among males due to delayed diagnosis and increased tumor growth before detection [18, 58].

Table (6): Comparison of Gender Distribution (coded:1=Male, 2= Female) Across Pituitary Tumor Subtypes Using ANOVA*

	Types of Tumors	mean ± Std. Deviation	Number of cases	P-value
Gender for all	Microadenoma	1.98 ± 0.151	44	< 0.001 **
	Macroadenomas	1.42 ± 0.502	31	
	Non-adenomas	1.68 ± 0.476	25	
	Total	1.73 ± 0.446	100	
	Overall Cases%		100%	

Fig 3 Microadenomas display a sharp female dominance (95.5%), whereas macroadenomas show a relatively balanced distribution (male 58%, female 41.9%). Non-adenomatous lesions lean slightly toward female predominance (68% vs. 32%). The visual pattern reinforces the statistical outcome of ANOVA and highlights gender disparities in pituitary pathology presentation and detection timing [59, 60].

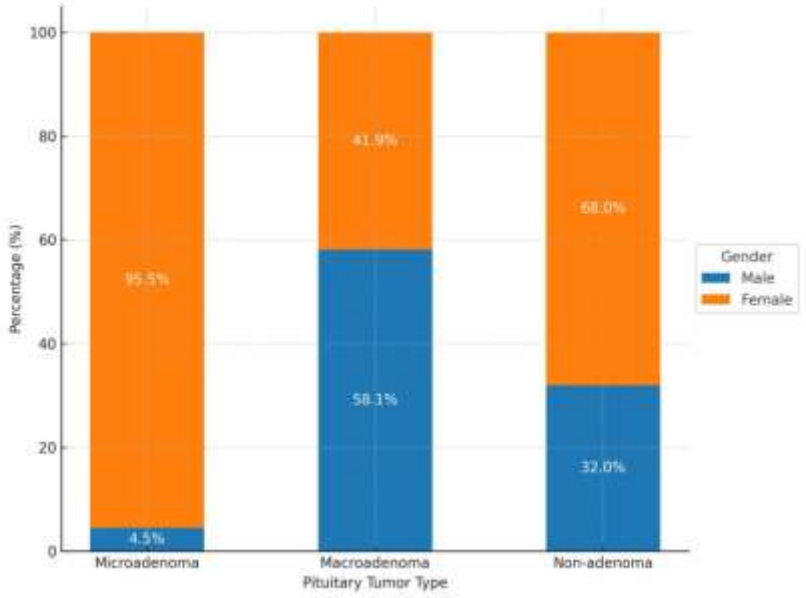

Fig (3): Stacked Bar Chart Representing Gender Distribution (Male and Female) Among Different Pituitary Tumor Types.

Table 7 The findings show that patients with macroadenomas had the highest mean age (39.25 ± 5.69 years), followed by non-adenoma cases (29.92± 7.40 years) and MIA (29.50 ± 4.60 years). The statistical significance (p< 0.001) indicates a meaningful age-related distribution among tumor types, with MA more prevalent in older individuals. This age disparity suggests a potential progressive nature of adenoma growth or delayed detection in MA cases, which has been previously highlighted in endocrinological literature [61].

Table (7): Comparison of Mean Age (Years) Among Pituitary Tumor Subtypes Using ANOVA

	Types of Tumors	Mean Age ± Std. Deviation (Years)	Number of cases	P-value
All Age (years)	Microadenoma	29.50 ± 4.60	44	< 0.001 **
	Macroadenomas	39.25 ± 5.69	31	
	Non-adenomas	29.92 ± 7.40	25	
	Total	32.64 ± 7.228	100	
	Overall Cases%		100%	

Fig 4 illustrates the distribution of mean ages with standard deviations (black bars) across tumor types and their respective case percentages. The visual clearly reflects the older average age associated with macroadenomas, reinforcing the statistical output from Table 7. The clustering of younger ages in microadenoma and non-adenoma groups supports the theory that smaller or non-adenomatous pituitary changes are detected earlier, especially in symptomatic individuals or during incidental imaging [62].

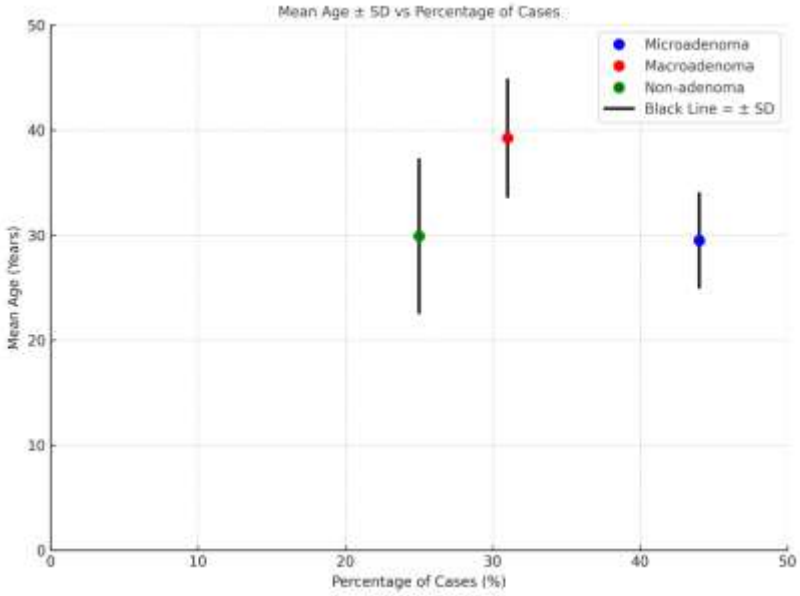

Fig (4): Scatter Plot Illustrating the Relation Between Mean Age (± Std. Deviation) and Percentage Distribution of cases Across Different Pituitary Tumor Subtypes (Microadenoma, Macroadenomas, Non-adenomas).

Table 8 demonstrates that visual disturbances were most prevalent among patients with macroadenomas, who had the lowest mean visual disturbance scores (1.13 ± 0.34), compared to those with MIA and non-adenomatous lesions (2.00 ± 0.00 for both groups). The statistically significant difference ($p < 0.001$) highlights the greater propensity for MA to compress the optic chasm or adjacent visual pathways, leading to more severe visual dysfunction [63, 64].

Table (8): Distribution of Visual Disturbances Scores Among Pituitary Tumor Subtypes with Statistical Significance

	Types of Tumors	mean ± Std. Deviation	Number of cases	P-value
Vision Disturbance Status	Microadenoma	2.00 ± 0.00	44	<0.001**
	Macroadenomas	1.13± 0.34	31	
	Non-adenomas	2.00 ± 0.00	25	
	Total mean	1.73 ± 0.44	100	
	Overall Cases%		100%	

Fig 5 graphically reinforces the tabulated data, showing that patients with MA had markedly lower mean visual disturbance scores compared to microadenomas and non-adenomatous lesions. The visual gap between groups further underscores the statistically significant findings ($p < 0.001$) and the clinical relevance of tumor size and extension in predicting visual outcomes [65, 66, 67].

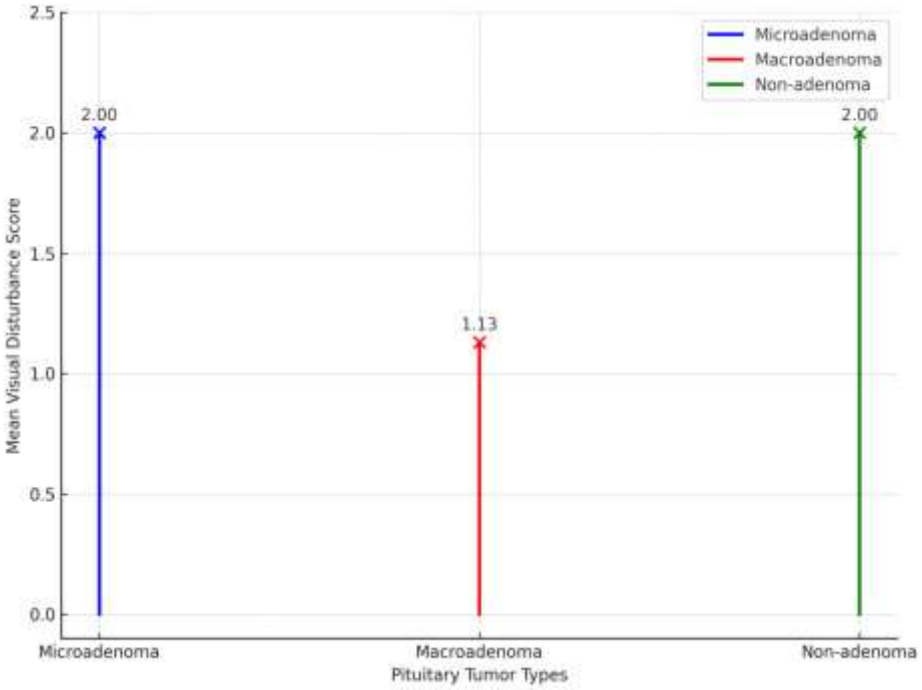

Fig (5): Lollipop Chart Depicting Mean Visual Disturbance Scores (± Std. Deviation) Across Pituitary Tumor Subtypes

Table 9 highest prolactin elevation macroadenomas findings, among the 18 male patients diagnosed with macroadenomas, 13 (72.2%) exhibited severe prolactin elevation, while 5 (27.8%) had moderate elevation. This aligns with current evidence that MA, particularly prolactinomas, often result in compression of the pituitary stalk or directly secrete prolactin, causing hyperprolactinemia. Studies confirm that macroadenomas cause increased prolactin levels by disrupting dopamine inhibition from the hypothalamus [19]. Such elevation often serves as a biochemical hallmark of functional macroadenomas, aiding early diagnosis and monitoring of treatment response. In contrast, non-adenomatous tumors presented an entirely different hormonal behavior, with 100% (8/8) of cases having normal prolactin levels. This suggests that these tumors are either non-secretory in nature or do not interfere with the hypothalamic–pituitary axis significantly, reaffirming their classification as non-functional lesions [64]. MIA, surprisingly, were underrepresented in this cohort, with only one case identified, yet it showed severe elevation, implying that even small tumors may exhibit secretory potential in certain contexts. However, their minimal presence limits statistical conclusions. Overall, the data strongly support the clinical utility of prolactin measurement as a differentiating tool between functional and non-functional pituitary lesions in male patients. Elevated prolactin, particularly at severe levels, should raise suspicion for MA, whereas normal levels are more suggestive of non-adenomatous tumors [28].

Table (9): Crosstabulation of Prolactin Levels and Pituitary Tumor Types in Male Patients (Chi-Square Test)

Tumor type of the Pituitary	Hormone(ng/mL) Prolactin Level for Male				Total cases	Asymptotic Significance (2 sided)
	Normal Prolactin	Mild elevated	Moderate elevated	Severe elevated		
Microadenoma	0	1	0	0	1	P<0.001**
Macroadenomas	0	0	5	13	18	
Non-adenomas	8	0	0	0	8	
Total	8	1	5	13	27	

Fig 6 illustrates the distribution of serum prolactin levels among male patients with pituitary tumors. The highest proportion of patients (48.1%) exhibited severe prolactin elevation, which corresponds to the majority of macroadenomas cases, indicating a strong functional profile and hormonal activity. Moderate elevation

accounted for 18.5%, also aligning with macroadenomas, supporting the hypothesis that even in the absence of extreme hyperprolactinemia, macroadenomas remain a major cause of hormonal disturbance. Normal prolactin levels were seen in 29.6% of patients, which corresponds almost entirely to non-adenomatous lesions, reaffirming their non-functional behavior. Only 3.7% of the patients showed mild elevation, suggesting that mild increases are rare and may be incidental or represent early-stage dysfunction.

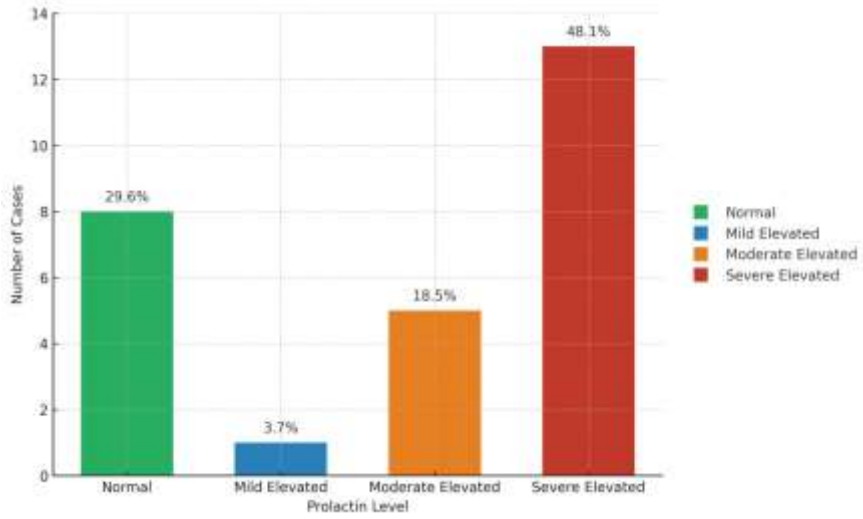

Fig (6): Stacked Bar Chart Depicting the Distribution of Prolactin Hormonal Levels Across Pituitary Tumor Types in Male Patients

Table 10 demonstrates a significant association between prolactin levels and pituitary tumor types in females ($p < 0.001$). All MIA cases (43/43, 100%) showed mild prolactin elevation, reflecting their typical presentation as prolactin-secreting tumors in women, often detected early due to reproductive symptoms. In contrast, macroadenomas showed moderate to severe elevations (100% of cases), with 61.5% exhibiting severe levels indicating greater tumor burden and higher secretory activity. Non-adenomatous tumors, comprising 23.3% of cases, showed 100% normal prolactin levels, confirming their non-functional nature .These findings emphasize the role of serum prolactin as a non-invasive tool to distinguish tumor behavior in female patients [51].

Table (10): Association Between Prolactin Levels and Pituitary Tumor Types in Female Patients: Crosstabulation with- (Chi-Square Tests, n=73**)**

Tumor type of the Pituitary	Hormone Prolactin Level for Female				Total cases	Asymptotic Significance (2 sided)
	Normal Prolactin	Mild elevated	Moderate elevated	Severe elevated		
Microadenoma	0	43	0	0	43	P<0.001**
Macroadenomas	0	0	5	8	13	
Non-adenomas	17	0	0	0	17	
Total	17	43	5	8	73	

Fig 7 displays the distribution of pituitary tumor types among female patients according to serum prolactin levels. The data reveals that 58.9% of cases fall under mild elevation, reflecting the dominance of microprolactinomas, which are often detected early due to menstrual or reproductive disturbances. Meanwhile, 23.3% showed normal prolactin levels corresponding to non-functioning tumors while only 11.0% had severe elevation, most likely due to macroadenomas. This hormonal pattern underscores the clinical relevance of prolactin screening in females, where mild elevations are diagnostic for functional MIA, often responsive to medical therapy [68].

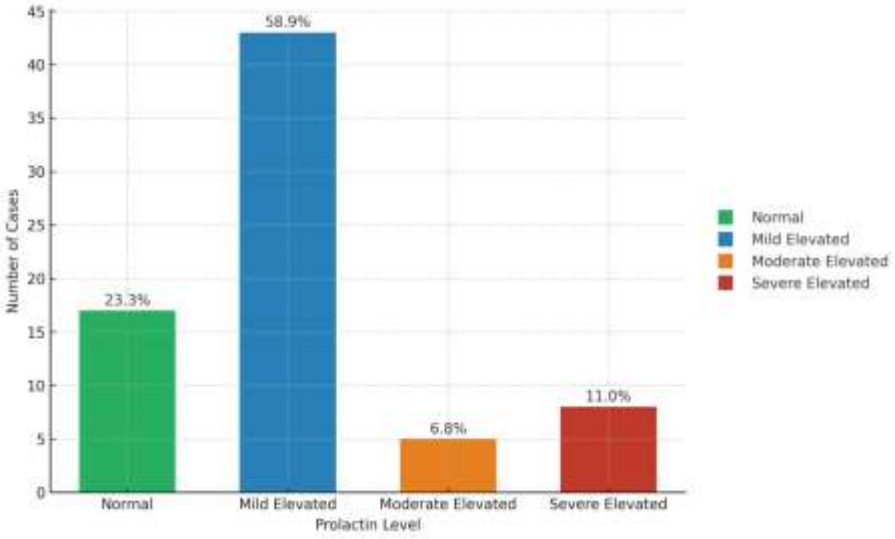

Fig (7): Distribution of Pituitary Tumor Types According to Prolactin Levels in Female Patients

Figs 8 presents comparative donut charts illustrating the proportional distribution of pituitary tumor types among male and female patients with hyperprolactinemia. In male patients 8A, macroadenomas were the predominant type, accounting for 66.7%, followed by non-adenomas (29.6%) and a minimal presence of microadenomas (3.7%). This suggests that men tend to present with larger, more invasive tumors likely due to delayed diagnosis or asymptomatic progression in early stages in contrast, female patients 8B, showed a predominance of microadenomas (58.9%), with macroadenomas at 17.8% and non-adenomatous tumors comprising 23.3%. This gender-specific distribution reflects earlier detection in women due to reproductive symptoms and routine hormonal evaluation. These patterns support the concept that tumor type and size are influenced by biological sex, hormonal sensitivity, and symptom-driven diagnosis, aligning with global epidemiological trends in pituitary adenomas [62, 69].

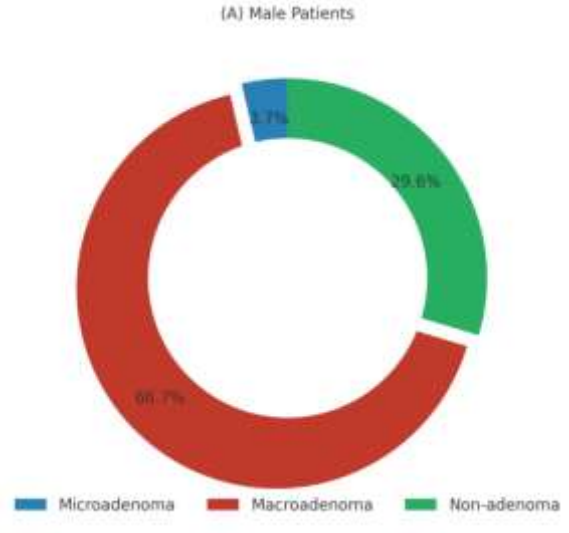

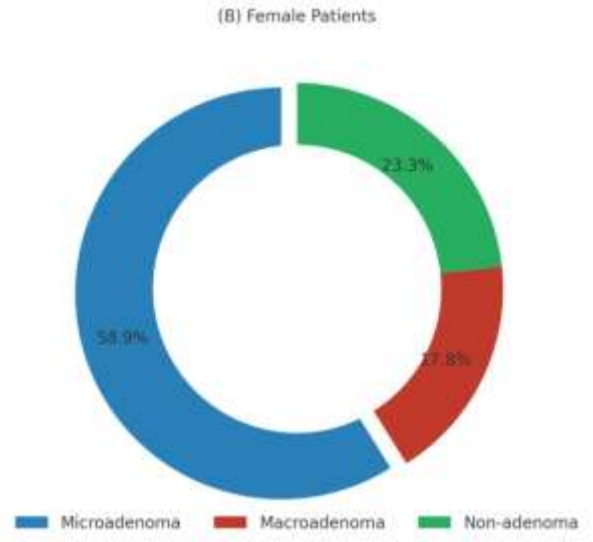

Figs (8): Comparative Detached Donut Charts Illustrating the Proportional Distribution of Microadenomas, Macroadenomas, and Non-Adenomatous Maas in Male and Female Patients with Hyperprolactinemia. **A.** Distribution of pituitary tumor types among male patients. **B.** Distribution of pituitary tumor types among female patients.

Table 11 shows a statistically significant relationship between menstrual cycle classification and pituitary tumor subtype in female patients ($p < 0.001$), highlighting how reproductive patterns correlate with tumor functionality. The highest frequency (58.9%) was observed in patients with irregular menstrual cycles, all of whom (43/43) were diagnosed with microadenomas. This confirms that mild prolactin elevation due to MIA disrupts the hypothalamic-pituitary-gonadal (HPG) axis, commonly leading to Oligomenorrhea or cycle irregularity. The second highest group (11.0%) included patients who had never experienced menstruation (primary amenorrhea), all linked to macroadenomas, likely due to significant prolactin excess from large tumors interfering with Gonadotropin-Releasing Hormone (GnRH) secretion. Meanwhile, normal cycles (23.3%) were exclusively seen in non-adenomatous tumors, supporting their non-functional profile and minimal hormonal disruption. The least represented group were those with no cycle for >3 months (6.8%), all of whom also had MA, indicating progression from irregularity to complete amenorrhea as tumor size and prolactin levels increase [70, 71].

Table (11): Cross-Tabulation Association Between Menstrual Cycle Classifications and Pituitary Tumor subtypes in Female Patients (Chi-Square Analysis, n=73)

Menstrual pattern classification	Tumor Type Female			Total	Asymptotic Significance (2-Sided)
	Microadenoma	Macroadenomas	Non- Adenomas		
Normal cycle	0	0	17	17	P<0.001**
Irregular cycle	43	0	0	43	
No cycle >3 months	0	5	0	5	
Never had menses	0	8	0	8	
Total	43	13	17	73	

Fig 9 displays a stacked bar chart representing the distribution of menstrual patterns among female patients diagnosed with pituitary tumors. The most prominent menstrual abnormality was irregular cycle, comprising 58.9% of the cohort (43 out of 73 patients). This pattern strongly correlates with microadenomas, which are commonly associated with mild-to-moderate hyperprolactinemia that disrupts the pulsatile release of GnRH, leading to Oligomenorrhea or cycle irregularity. The second most common category was normal cycle (23.3%), mostly seen in non-functioning tumors (non-adenomas), which do not alter the hypothalamic-pituitary-gonadal (HPG) axis. A smaller portion (11.0%) had never experienced menses (primary amenorrhea), which is typically seen in patients with macroadenomas diagnosed early in adolescence or with significant hormonal

disruption. The least represented group (6.8%) had no cycle for >3 months, a feature suggestive of secondary amenorrhea, also linked to macroprolactinomas and sustained prolactin elevation [24, 72].

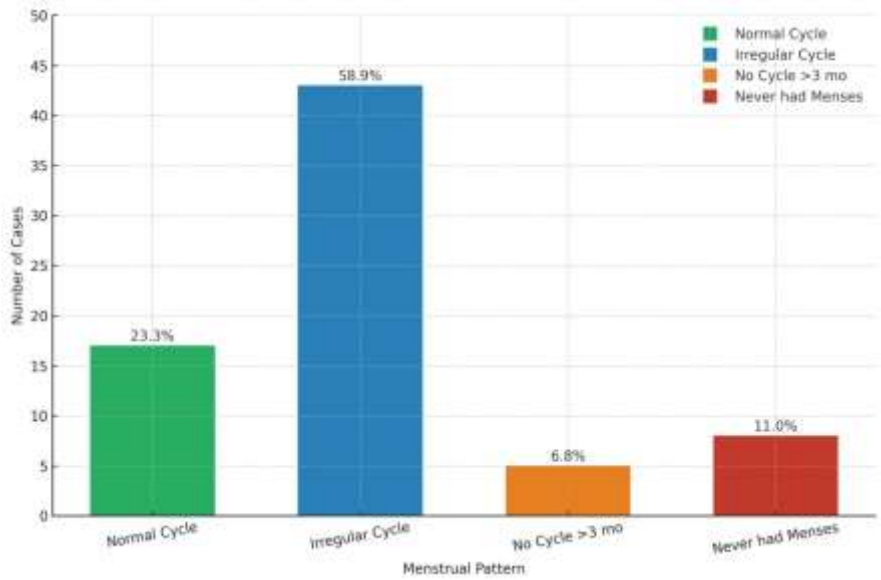

Fig (9): Stacked Bar Chart Illustrating Menstrual Pattern Distribution Across Pituitary Tumor Types in Female Patients

Table 12 displays the distribution of Galactorrhea severity among 27 male patients with pituitary tumors. Surprisingly, 48.1% of males exhibited severe Galactorrhea (+++), a rare but highly indicative sign of macroprolactinomas or functionally active tumors secreting high levels of prolactin. Only 18.5% reported mild Galactorrhea, while 33.3% had no Galactorrhea .Importantly, no patients had moderate (++ grade) Galactorrhea, revealing a polarized distribution between absent and severe symptoms. These findings align with evidence that male Galactorrhea, though uncommon, is strongly linked to high prolactin levels, often exceeding 200 ng/mL, and is more likely associated with larger and symptomatic adenomas [28, 73].

Table (12): Distribution Frequency Galactorrhea Male patients

Galactorrhea Levels Male	Frequency	Valid Percent
No Galactorrhea	9	33.3
Mild +Galactorrhea	5	18.5
Moderate++ Galactorrhea	0	0.0
Severe +++ Galactorrhea	13	48.1
Total	27	100.0

Fig 10 showing a bar chart of Galactorrhea levels among male patients. The highest bar represents severe Galactorrhea (48.1%) . The second largest group is those with no Galactorrhea (33.3%.) Mild cases (18.5%) appear in lower frequency, and moderate cases are entirely absent This bimodal pattern visually confirms that Galactorrhea in men tends to be either absent or highly severe, with minimal intermediate expression. This clinical presentation may help prioritize hormonal testing and MRI in symptomatic males [63, 74].

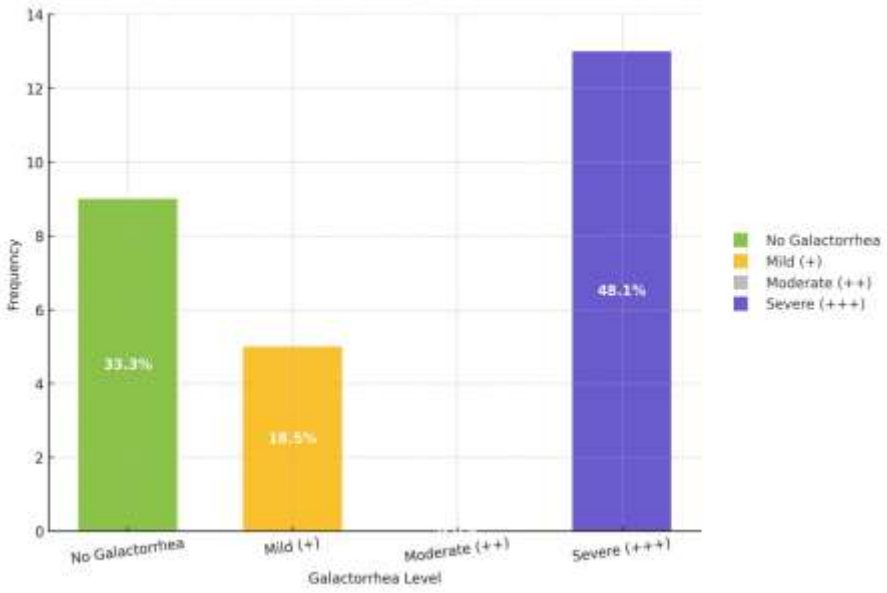

Figure (10): Frequency and Percentage Distribution Galactorrhea Levels Among Male Patients with Pituitary Mass tissues

Table 13 presents the distribution of Galactorrhea severity among 73 female patients with pituitary lesion. The data reveal that, 58.9% of the women exhibited mild Galactorrhea, indicating its common occurrence as an early and sensitive marker of microprolactinoma 23.3% had no Galactorrhea, likely representing non-functional or non-adenomatous tumors. Only 6.8% showed moderate (++ level) Galactorrhea, and 10.8% had severe (+++) Galactorrhea, suggestive of macroadenomas with higher prolactin secretion. This distribution confirms that Galactorrhea is a hallmark symptom in females with functional pituitary tumors, often preceding other hormonal or imaging findings. Its grading correlates with tumor size and prolactin level, with more severe forms typically seen in macroadenomas [23, 75, 76].

Table (13): Distribution Frequency Galactorrhea Female patients

Galactorrhea Levels Female	Frequency	Valid Percent
No Galactorrhea	17	23.3
Mild +Galactorrhea	43	58.9
Moderate ++Galactorrhea	5	6.8
Severe +++ Galactorrhea	8	10.8
Total	73	100.0

Figure 11 is a bar chart illustrating the percentage and frequency of Galactorrhea levels among female patients. The dominant bar (orange) represents mild Galactorrhea (58.9%), visually confirming its high prevalence. The blue bar (10.8%) marks severe Galactorrhea, associated with larger tumors. Moderate levels (6.8%) are relatively rare, indicating that symptom progression may shift quickly from mild to severe as tumor size increases. 23.3% of patients are symptom-free, aligned with non-functional tumor types. This chart visually supports the clinical understanding that mild Galactorrhea is the earliest and most frequent expression of hyperprolactinemia in females, while severe levels are less common but more diagnostically specific [37, 63].

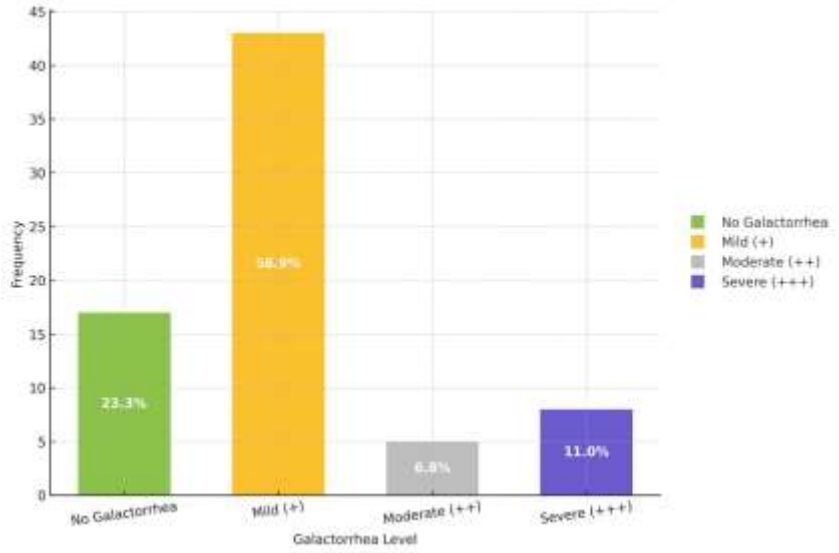

Figure (11): Bar-Chart Representing the Frequency and Valid Percentages of Different Galactorrhea Severity Levels (No, Mild, Moderate, Sever) in Female Patients with Pituitary Mass Tissues

Table 14 provides most patients (58.9%) were diagnosed with microadenomas, presenting with mild Galactorrhea, mild prolactin elevation, and irregular menstrual cycles. This profile aligns with early-stage functional microprolactinomas, which often maintain partial gonadotropic feedback Moderate to severe Galactorrhea was observed exclusively in macroadenomas (17.7% combined), accompanied by moderate to severe prolactin elevation, and associated with more severe menstrual disturbances including amenorrhea or absence of menses for over 3 months. These findings reflect greater hormonal disruption due to tumor size and mass effect. Patients with non-adenomatous lesions (23.3%) exhibited normal prolactin levels, absence of Galactorrhea, and regular menstrual cycles, indicating their non-functional nature and minimal impact on the hypothalamic pituitary gonadal axis [77, 78, 79].

Table (14): Clinical and Hormonal Characteristics Among Female Patients

Tumor type of the Pituitary Gland	Galactorrhea Status	Prolactin Level	Menstrual Status	Frequency	Percent
Microadenoma	Mild + Galactorrhea	Mild elevation	Irregular cycle	43	58.9%
Macroadenomas	Moderate++ Galactorrhea	Moderate elevation	No cycle ≥3 months	5	6.8%
Macroadenomas	Sever+++ Galactorrhea	Sever elevation	Never had menses	8	10.9%
Non-adenomas	No Galactorrhea	Normal	Regular cycle	17	23.2%
Total				73	100%

Fig 12 illustrates the distribution of Galactorrhea severity (mild, moderate, severe) among female patients with pituitary lesions. The chart reveals that 58.9% of cases exhibited mild Galactorrhea, indicating its high prevalence as an early marker of hormonal disruption, particularly in microadenomas. Severe forms of Galactorrhea were observed in 10.8% of patients, suggesting a stronger correlation with macroadenomas, where elevated prolactin levels and tumor size interfere significantly with the hypothalamic-pituitary axis. Notably, 23.3% of patients had no Galactorrhea, a distribution consistent with non-functioning adenomas or non-adenomatous lesions that do not secrete prolactin. This visual presentation aligns with the clinical understanding that mild Galactorrhea often precedes other symptoms and is more frequently associated with smaller tumors (e.g., microadenomas), while severe symptoms reflect progression or macroadenomas pathology. The rarity of moderate Galactorrhea (6.8%) suggests a rapid clinical transition from mild to severe stages in hormonally active lesions [62, 26, 79, 80].

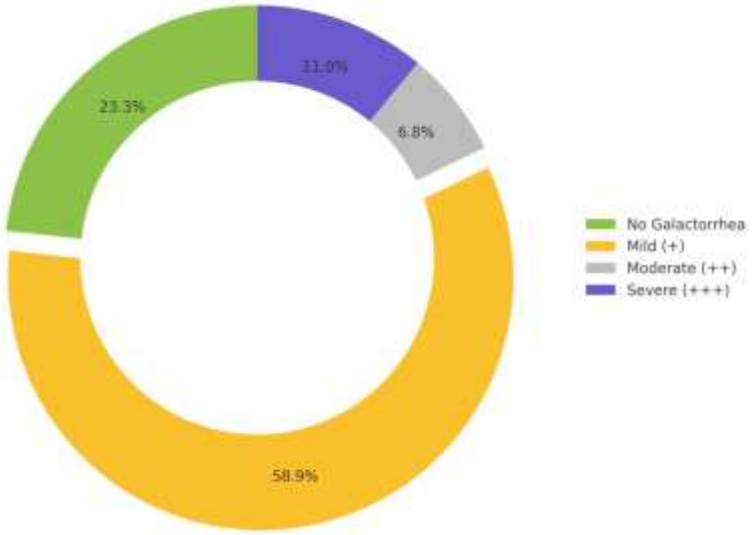

Figure (12): Exploded Donut Chart Illustrating the Severity of Galactorrhea (mild, moderate, sever) According to Menstrual Irregularities and Tumor Classification in Female Patients Diagnosed with Pituitary mass tissues

Table 15 reveals the clinical distribution of Galactorrhea and prolactin levels in male patients with pituitary tumors. Notably, 48.1% of male patients exhibited severe (+++) Galactorrhea, all of whom had macroadenomas with marked prolactin elevation, supporting previous findings that Galactorrhea is a rare but significant symptom in men, typically reflecting advanced functional adenomas with aggressive secretion patterns [24]. Conversely, 29.6% of male patients showed no Galactorrhea and normal prolactin, corresponding to non-adenomatous lesions or non-functioning tumors, aligning with the hypothesis that Galactorrhea in men is almost exclusively a result of hormonally active pituitary pathology [50]. The remaining 18.5% had mild Galactorrhea with mild prolactin elevation, often seen in early macroadenomas or less invasive prolactinomas. This hormonal-Galactorrhea profile in males underscores the diagnostic utility of Galactorrhea in distinguishing tumor functionality and progression, although it remains underreported due to lower sensitivity in men compared to women [28, 81].

Table (15): Clinical and Hormonal Characteristics Among Male Patients

Tumor type of the Pituitary gland	Galactorrhea Status	Prolactin Level	Frequency	Percent
Microadenoma	No Galactorrhea	Mild elevation	1	3.7%
Macroadenomas	Mild +Galactorrhea	Mild elevation	5	18.5%
Macroadenomas	Sever +++Galactorrhea	Sever elevation	13	48.1%
Non-adenomas	Absent	Normal	8	29.6%
Total			27	100%

Fig 13 presents an exploded donut chart illustrating the distribution of Galactorrhea and prolactin levels among male patients with pituitary tumors based on tumor type. The chart highlights that 48.1% of patients with macroadenomas presented with severe (+++) Galactorrhea and significantly elevated prolactin levels, reflecting the aggressive secretory nature of these tumors. This finding is consistent with studies showing that MA in males often manifest with more severe hyperprolactinemia and clinical symptoms due to delayed diagnosis [24] .In contrast, 29.6% of patients were diagnosed with non-adenomatous lesions and exhibited neither Galactorrhea nor prolactin abnormalities, supporting the concept that non-functioning lesions are typically hormonally silent [64]. Additionally, 18.5% had mild Galactorrhea with mild prolactin elevation possibly representing the early phase of macroadenomas or partially functioning tumors [81]. Only 3.7% of cases were microadenomas with mild hormonal and symptomatic profiles, reaffirming their lower clinical impact unless incidentally discovered.

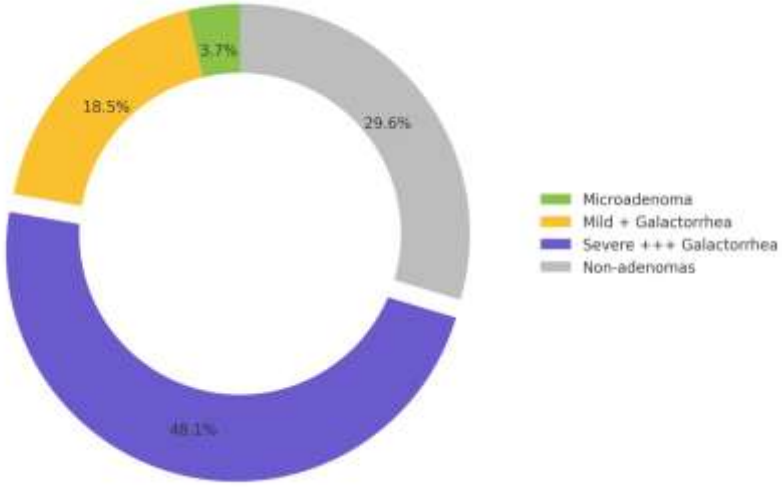

Fig (13): Exploded Donut Chart Distribution of Galactorrhea and Prolactin Levels Among Male Patients with Pituitary mass tissues According to Tumor Type.

Table 16 demonstrates a statistically significant difference ($p < 0.001$) in pre-contrast T1-WI-SE MRI signal intensities among various pituitary tumor types, confirmed by a strong effect size ($Eta^2 = 0.625$). Non-adenomatous lesions predominantly exhibited iso to hypointense signals with a notably high mean score of 3.0 ± 0.0, likely reflecting their heterogeneous content or cystic/vascular components. In contrast, microadenomas and macroadenomas consistently showed iso to hypointense signals, with lower mean values ranging from 1.0 to 1.5, suggesting a more homogeneous soft-tissue density and lack of internal hemorrhage or cysts. Notably, 10 cases of MA displayed hypointense signal with contour distortion, indicating possible invasion or compression effects on an important radiological feature associated with aggressive growth patterns and mass effect on surrounding structures such as the optic chiasm [82, 83].

Table (16): Quantitative Analysis of Pre-contrast T1-WI MRI Signal Intensities Across Pituitary Tumor Types with ANOVA Significance and Effect Size

Tumor Type of the Pituitary Gland	pre-contrast T1-Weighted image Signal	mean ± Std. Deviation	Number of cases	Point estimate	P-value
Non-adenomas	Iso-hypo signal intensity	3.0 ± 0.0	25	0.625	<0.001**
Microadenoma	Hypo signal intensity	1.5 ± 0.49	22		
Microadenoma	Iso-signal intensity	1.0 ± 0.0	12		
Microadenomas	hypo signal intensity with possible contour distortion	1.0 ± 0.0	10		
Macroadenomas	hypo signal intensity	1.0 ± 0.0	31		
Total		1.81 ± 0.81	100		
Eta-squared					

Fig 14 visually represents the distribution of pre-contrast T1-WI signal intensities among different pituitary tumor types. The bar chart demonstrates that non-adenomatous lesions have the highest mean signal intensity (≈3.0), accounting for 29% of cases. In contrast, MA showed consistently hypointense signals,

representing 31% of the sample. This hypo signal intensity is strongly associated with high cellularity and reduced water content, typical of solid adenomatous tissue. Similarly, MIA presented with variable signals ranging from hypointense (22%) to iso-intense (12%) indicating potential differences in their Histopathological architecture. A smaller fraction (10%) of MIA exhibited distorted hypointense signals, often correlating with invasive growth or local distortion. This signal variation aligns with literature indicating that non-functional tumors and larger macroadenomas tend to demonstrate low to intermediate intensity on T1-WI, while non-adenomatous lesions tend to have atypical, sometimes hyperintense features due to internal complexity [84].

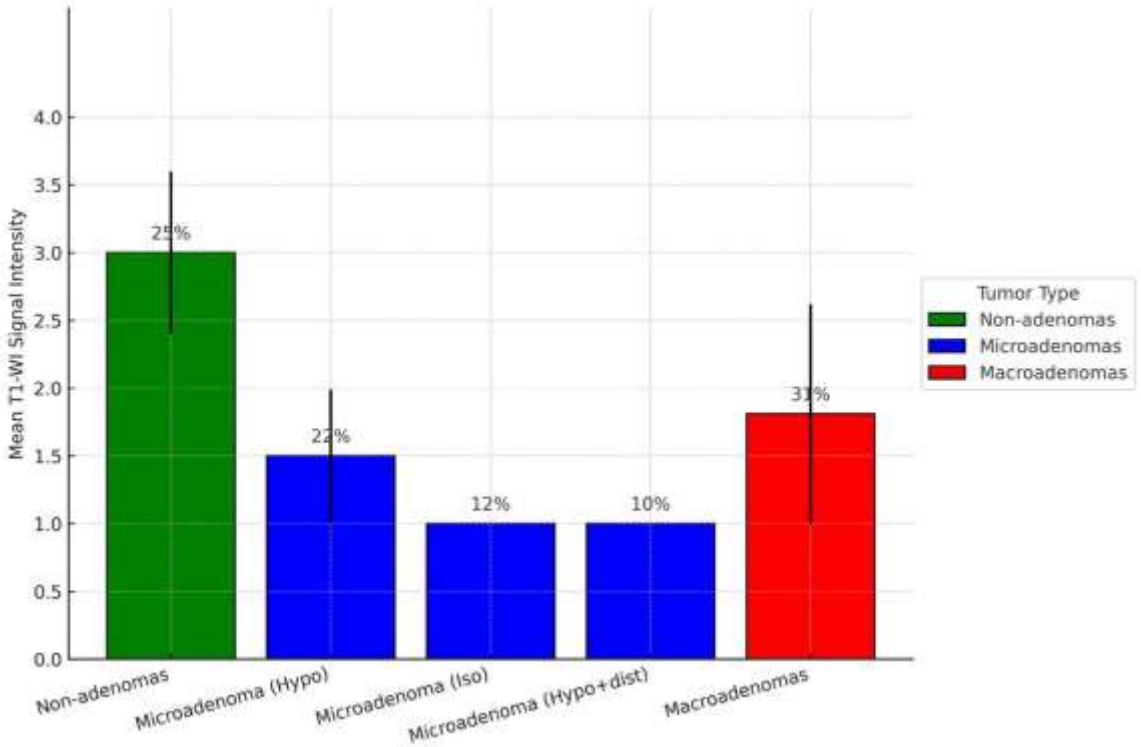

Fig (14): Bar Chart Illustrating the Mean Pre-contrast T1-WI Signal Intensity (± Std. Deviation) Across Pituitary Tumor Subtypes with Percentage Distribution of cases

Table 17 illustrates the comparative T2-WI MRI signal intensity across various pituitary tumor subtypes using ANOVA. Notably, non-adenomatous lesions exhibited the highest mean signal intensity (2.0 ± 0.0), while MA consistently demonstrated a low and homogeneous hyperintense T2 signal (1.0 ± 0.0), suggesting solid, less hydrated tumor content. Microadenomas revealed more diverse T2 features, ranging from iso-hyper (1.8 ± 0.49) to mildly hyperintense (1.5 ± 0.49), and even focal iso-hyper signal patterns with contour irregularities (1.2 ± 0.30), possibly reflecting cystic degeneration, fibrosis, or hemorrhage. The ANOVA yielded a statistically significant difference ($p < 0.001$), confirming that T2 signal heterogeneity is more prominent in MIA, whereas MA are typically more uniform [85].

Table (17): Comparative Analysis of T2-Weighted Image MRI Signal Intensity Across Microadenoma, Macroadenomas, and Non-adenomas Cases Using ANOVA Test

Types of Tumors	T2-WI Signal on MRI	mean ± Std. Deviation	Number of cases	Point estimate	P-value
Non-adenomas	Iso-hyper signal intensity	2.0 ± 0.0	25		
Microadenoma	Iso-hyper signal intensity	1.8 ± 0.49	22	0.654	<0.001**
Microadenoma	Iso-mild hyper signal intensity	1.5 ± 0.49	12		
Microadenoma	Focal iso-hyper signal intensity	1.2 ± 0.30	10		

Macroadenomas	Hyper signal intensity	1.0 ± 0.0	31		
Total		2.01 ± 0.91	100		

Eta-square

Fig 15 presents a comparative analysis of mean T2-WI signal intensities across pituitary tumor subtypes. Non-adenomas demonstrated the highest mean intensity (2.0, 25%), followed by microadenomas with variable signal patterns: iso-hyperintense (1.8, 22%), iso–mild hyper (1.5, 12%), and focal iso-hyper (1.2, 10%). MA showed consistently low signal intensity (1.0) despite constituting the largest proportion (31%) of cases. This variability in T2 signal among microadenomas may reflect differing tumor cellularity, vascularization, and cystic components [71, 86].

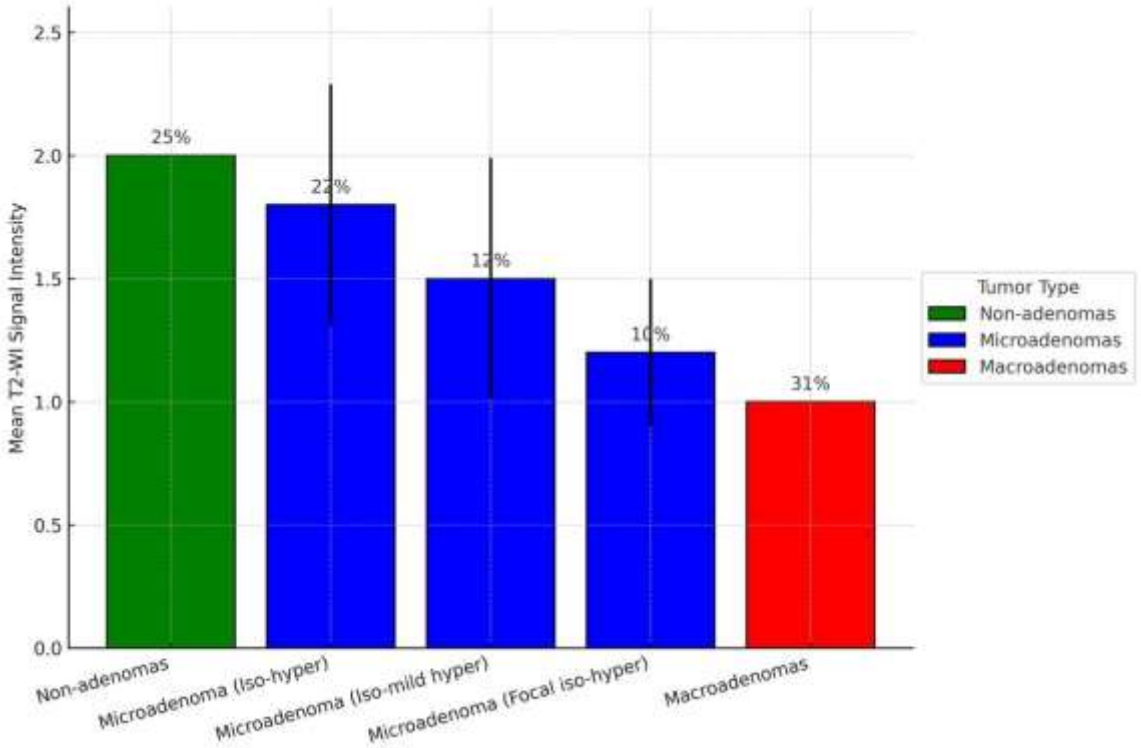

Fig (15): Comparative Analysis of Mean T2-Weighted Image MRI Signal Intensity (± Std. Deviation) Across Pituitary
Tumor Subtypes with Percentage Distribution of Cases

Table 18 The cohort shows a T2-WI predominance of iso-to-hyperintense signals: iso-hyper accounts for 47%, frankly hyper for 31%, and iso-mild hyper for 12% (→ 90% of T2 signals trend ≥iso), with a smaller focal iso-hyper subset (10%). This distribution fits classic pituitary imaging: adenomas and many non-adenomatous seller lesions. iso- to hyperintense on T2 due to higher water content/less collagen. On pre-contrast T1-WI, hypo signal intensity dominates (53%), followed by iso-hypo (25%), iso (12%), and hypo + contour distortion (10%), which is typical for solid adenomatous tissue and highlights cases where mass effect/invasion is suspected (contour distortion). Together, these patterns reinforce the practical rule: T1 hypo signal intensity + T2 iso/hyper strongly suggests pituitary adenoma, while deviations (e.g., marked heterogeneity or distortion) cue to radiologists consider non-adenomatous lesions or aggressive behavior and to correlate with clinical/endocrine data [38, 82, 87].

Table (18): Comparative Distribution of Signal Intensity Patterns on pre-contrast T1-and T2 Weighted MRI Sequences in the Study Cohort

Modality	Signal type	Frequency (n)	Percent (%)	Cumulative percent (%)
	Iso-hyper signal intensity	47	47.0	47.0

T2-WI	Hyper signal intensity	31	31.0	78.0
	Iso-mild hyper signal intensity	12	12.0	90.0
	Focal iso-hyper signal intensity	10	10.0	100.0
T1-WI	hypo signal intensity	53	53.0	53.0
	Iso- hypo signal intensity	25	25.0	78.0
	Iso-signal intensity	12	12.0	90.0
	hypo signal + contour distortion	10	10.0	100.0

Table 19 shows that heterogeneous enhancing lesions were most common (31%) and were predominantly T1 hypointense pre-contrast (mean score = 1.0), consistent with macroadenomas or lesions. Hypo-enhancing tumors formed 22%, again tracking with adenomas that enhance less than the normal gland on early dynamic phases. In contrast, homogeneous early enhancing (15%) and small delayed enhancing (12%) patterns likely reflect microadenomas that are conspicuous on dynamic T1+Gd because the normal gland enhances earlier/more intensely; focal delayed enhancing with contour distortion (10%, mean = 3.0) flags invasive/aggressive behavior. The overall association is significant ($p < 0.001$), supporting the diagnostic value of DCE-MRI for functional classification and conspicuity [87, 88, 89, 90].

Table (19): Dynamic Contrast Enhancement (T1+Gd) Patterns Stratified by pre-contrast T1-Weighted Signal Pattern: Mean± Std. Deviation. Case Distribution and Statistically Significant

Dynamic Contrast Enhancement (T1+Gd)	Signal T1-Weighted image pre-contrast	mean ± Std. Deviation	Frequency (n)	Percent	Cumulative	P-value
Normal physiological enhancing	Iso-hypo signal intensity	1.2 ± 0.30	10	10.0%	10.0%	<0.001**
Homogenous early enhancing	Iso-hypo signal intensity	1.3 ± 0.28	15	15.0%	25.0%	
Hypo enhancing	hypo signal intensity	1.5 ± 0.49	22	22.0%	47.0%	
Small delayed enhancing	Iso-signal intensity	1.0 ± 0.0	12	12.0%	59.0%	
Focal delay enhancing	hypo signal intensity with possible contour distortion	3.0 ± 0.0	10	10.0%	69.0%	
Heterogeneous enhancing	hypo signal intensity	1.0 ± 0.0	31	31.0%	100.0%	
Total		1.5 ± 0.18	100	1.00%	100.0%	
Overall Cases%			100 Cases			

Table 20 The distribution of dynamic gadolinium enhancement patterns on T1-weighted MRI reveals distinct profiles between pituitary tumor subtypes. MA predominantly exhibited heterogeneous enhancement (31%), reflecting their variable internal architecture, necrosis [91]. MIA frequently demonstrated Hypo enhancing patterns (22%) and small delay enhancement (12%), aligning with delayed contrast uptake was linked to reduced vascularity and altered capillary permeability [92]. Non-adenomatous lesions were more likely to show normal physiological (10%) and homogenous enhancement (15%) [93]. The statistical significance ($p < 0.001$) emphasizes the diagnostic potential of enhancement patterns in differentiating adenomatous from non-adenomatous lesions.

Table (20): Distribution of Dynamic Gadolinium Enhancement (T1+Gd) Values Across Pituitary Tumor Subtypes on T1-WI MRI

T1-Dynamic Contrast Enhancement (T1+Gd) Agent's study	Types of Tumors	mean ± Std. Deviation	Frequency (n)	Percent	Cumulative	P-value
Normal Physiological enhancing	Non-adenomas	3.2 ± 0.0	10	10%	10%	
Homogenous enhancing	Non-adenomas	3.0 ± 0.0	15	15%	25%	<0.001**
Hypo enhancing	Microadenoma	1.0 ± 0.0	22	22%	47%	
Small delay enhancing	Microadenoma	1.0 ± 0.0	12	12%	59%	
Focal delay enhancing	Microadenoma	1.0 ± 0.0	10	10%	69%	
Heterogeneous enhancing	Macroadenomas	2.0 ± 0.0	31	31	100%	
Total		1.8 ± 0.8	100	100%	100.0%	
Overall Cases%			100 cases			

Fig 16 illustrates the largest segment represents heterogeneous enhancement (31%), which is visually emphasized by separation from the donut chart to underscore its predominance. This pattern is most often associated with macroadenomas and aggressive lesions due to intratumoral necrosis [91]. Hypo enhancement accounts for 22% of cases, frequently linked to MIA, reflecting reduced perfusion and capillary permeability changes within these smaller lesions. Homogeneous enhancement (15%) and small delay enhancement (12%) are generally associated with benign and well-vascularized tumors, often correlating with stable endocrine profiles [92, 93]. Normal physiological enhancement (10%) is typically observed in non-adenomatous lesions, while focal delay enhancement (10%) often reflects localized tumor fibrosis or mass effect on vascular supply.

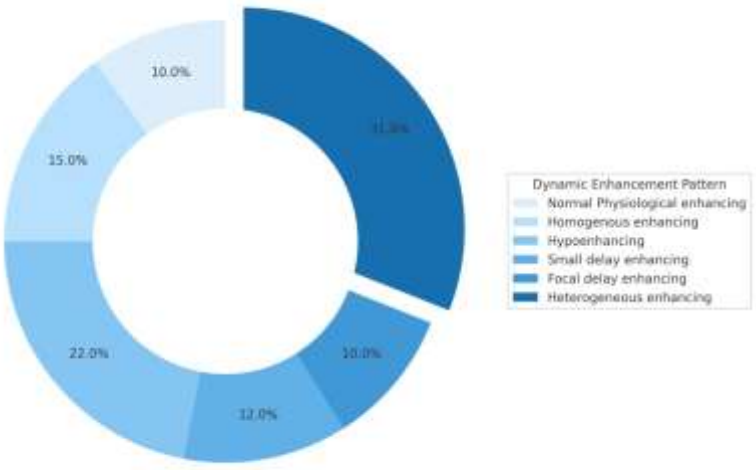

Fig (16): Exploded Donut Chart Distribution of Dynamic Contrast Enhancement (DCE) Patterns on T1-Weighted MRI in Pituitary mass Patients.

Table 21 The heterogeneous enhancement pattern was the most frequent overall (31%), with a marked predominance in the left anterior lobe (8 cases) and central/suprasellar region (5 cases). This pattern is often linked to macroadenomas or more aggressive lesions due to tumor vascular heterogeneity and necrotic areas, consistent with prior reports that heterogeneous contrast uptake correlates with tumor invasiveness and

histologic variability [91, 94]. Hypo enhancement accounted for 22% of cases, frequently localized to the left anterior lobe (7 cases) and central/suprasellar area (5 cases), which may indicate hypo vascular adenomas or those with dense fibrous stroma [80]. Normal physiological enhancement was observed in 18%, mostly in the normal scan group (11 cases), aligning with typical pituitary gland perfusion patterns【95]. Small delay and focal delay enhancement patterns (12% and 10%, respectively) were less common and were distributed across various locations, potentially reflecting early or localized vascular compromise. Homogeneous enhancement (15%) was mainly seen in the normal scan group (3 cases) and left anterior lobe (5 cases), suggesting benign and well-vascularized microadenomas [96]. The statistically significant p-value < 0.001 highlights a strong association between DCE-MRI pattern and tumor location, reinforcing that lesion vascularity and enhancement kinetics can be region-specific within the pituitary gland. This supports the role of dynamic MRI not only in detection but also in subregional characterization of pituitary lesions, aiding pre-surgical planning and differentiation between adenomas, normal variants, and other Sellar pathologies【91, 95, 96].

Table (21): Cross-tabulation of Dynamic Contrast Enhancement (T1+Gd) Patterns and Anatomical Localizations of Pituitary Masses on MRI Studies

Location mass of the Pituitary adenomas	Hypo	Small delay	Focal delay	Homogenous	Heterogeneous	Normal Physiological	Frequency (n)	P-value
Left anterior lobe	7	4	3	5	8	3	30	< 0.001**
Central, and Suprasellar	5	3	2	3	5	2	20	
Normal scan	3	2	2	3	4	11	25	
Compression Chiasm	3	1	1	2	3	1	11	
Right anterior lobe	2	1	0	1	2	1	7	
Central Pituitary	2	1	1	1	2	0	7	
Total	22	12	10	15	31	18	100	
Overall Cases%							100 Cases	

Fig 17 the left anterior lobe emerges as the most frequently involved region (~31%), with prominent Hypo enhancing and heterogeneous patterns consistent with macroadenomas that disrupt vascular supply and display internal heterogeneity. Central and suprasellar regions also show a high mix of hypo and small delay enhancement (~23%), suggesting variable tumor perfusion and microvasculature. Locations such as optic chiasm compression, right lobe, and central pituitary exhibit lower frequencies (<11%) but still reveal distinct enhancement signatures, emphasizing that regional anatomy influences vascular dynamics. Clinically, these findings underscore the importance of location-specific DCE profiling for instance, left anterior lobe lesions with heterogeneous enhancement may guide suspicion toward macroadenomas requiring a tailored surgical approach, whereas central suprasellar lesions with delayed enhancement may favor cautious follow-up [97, 98, 99, 100].

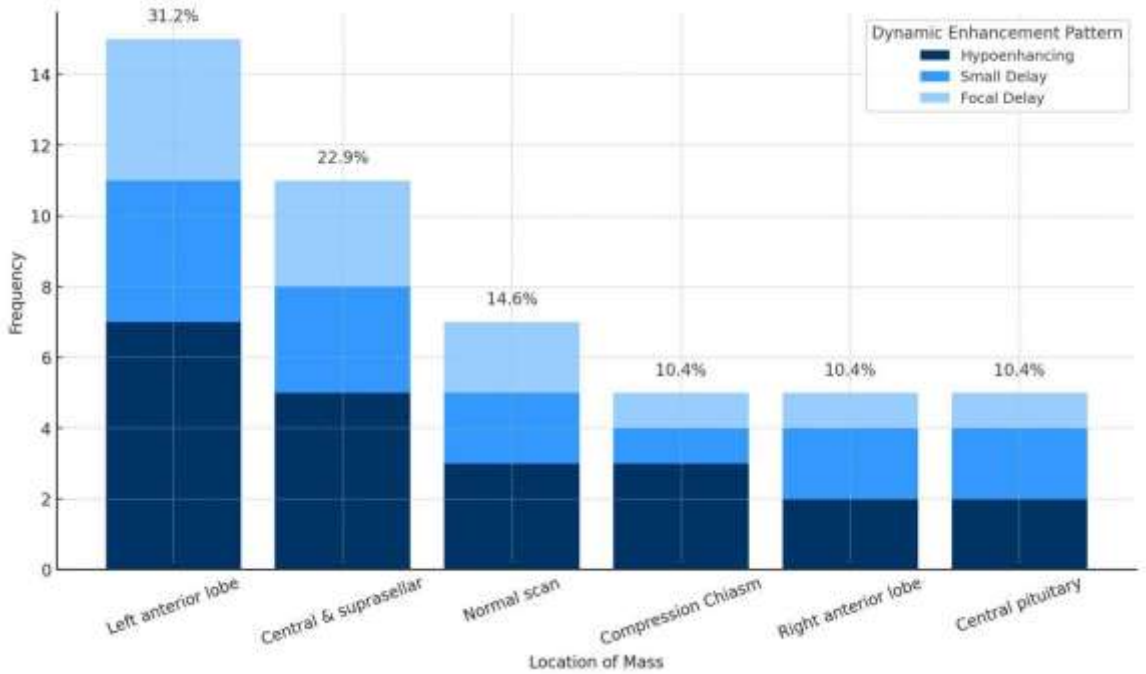

Fig (17): Stacked Bar Chart Showing the Distribution of Dynamic Contrast-Enhancement DCE-MRI (T1+Gd) Patterns Across Different Anatomical Locations of the Pituitary Gland.

Table 22 demonstrates a robust correlation between BMI category and DCE-MRI pattern in pituitary adenomas ($p < 0.001$). Heterogeneous/early heterogeneous enhancement dominates in the overweight/obesity strata, whereas hypo-enhancement is relatively more common in lower BMI (normal) categories. This gradient is biologically plausible: obesity is associated with microvascular remodeling, increased permeability, and pro-angiogenic signaling, which can translate radiologically into earlier and more heterogeneous enhancement on dynamic T1-WI. Conversely, more uniform hypo-enhancement aligns with lower perfusion or more fibrous/less vascular tissue, patterns often described in adenomas with lower micro vessel density. Clinically, these data suggest that patient adiposity may influence adenoma perfusion phenotypes on DCE-MRI, refining differential diagnosis and potentially informing surgical planning (e.g., anticipating soft, vascular tumors vs. firmer fibrotic lesions). Integrating BMI with DCE pattern alongside endocrine and morphologic features could improve pre-operative risk stratification [92, 98, 101].

Table (22): Cross Tabulation of WHO BMI Classifications and Dynamic Contrast Enhancement (T1+Gd) Pattern in Pituitary Adenomas: A statistical Correlation Study

Dynamic Enhancement Contrast (T1+Gd) Agent's study	Normal (n)	Overweight (n)	Obesity I (n)	Obesity II (n)	mean ± Std. Deviation	Frequency (n)	Cumulative Percent	P-value
Hypo enhancing	2	20	0	0	5.50 ± 9.71	22	22.0	< 0.001**
Early heterogeneous enhancing	2	14	9	6	7.75 ± 5.06	31	53.0	
Normal physiological enhancing	10	0	0	0	2.50 ± 5.00	10	63.0	
Homogenous early enhancing	12	2	0	1	3.50 ± 5.74	15	100.0	
Small delayed	4	6	2	0	3.00 ±	12	85.0	

enhancing					2.58			
Focal delayed enhancing	6	2	2	0	2.50 ± 2.52	10	73.0	
Total	36	44	13	7	4.50 ± 2.90	100		
Overall Cases%						100 Cases		

Fig 18 illustrates the distribution of Dynamic Contrast Enhancement (DCE) patterns on T1-WI MRI across different WHO BMI categories in patients with pituitary adenomas. The most prevalent enhancement pattern was early heterogeneous enhancement (31.0%), followed by Hypo enhancing lesions (22.0%). Both patterns showed a substantial representation among overweight and obese patients, suggesting a possible link between adiposity and tumor vascularization heterogeneity. In contrast, normal physiological enhancement accounted for only 10.0% of cases, predominantly in normal BMI individuals. This trend aligns with recent studies indicating that increased BMI may influence pituitary tumor angiogenesis and contrast uptake dynamics, potentially due to metabolic and hormonal alterations associated with obesity. The clear stratification of patterns by BMI categories underscores the potential role of patient metabolic status in modulating MRI enhancement characteristics, a finding with important implications for differential diagnosis and individualized imaging protocols [102, 103].

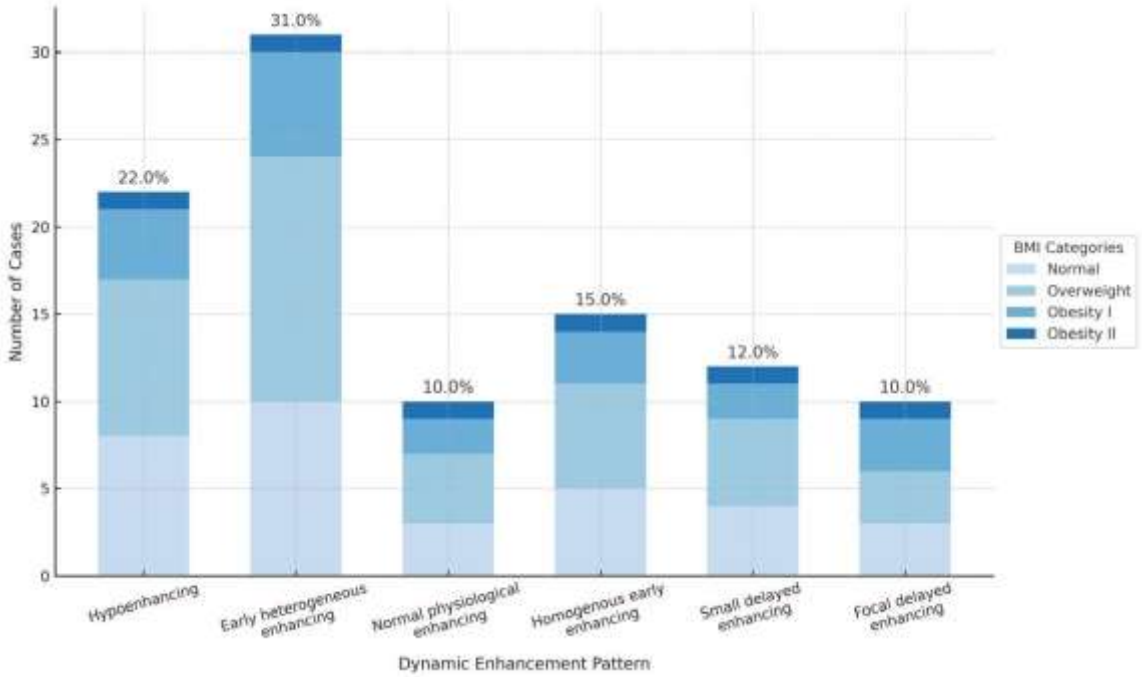

Fig (18): Distribution of WHO BMI Classifications Across Dynamic Contrast Enhancement (T1+Gd) Patterns in Pituitary Adenomas: A Statistical Correlation Analysis

Table 23 The comparative analysis of pituitary tumor types by anatomical location reveals that microadenomas most frequently involve the left anterior lobe (30%) and right anterior lobe (10%), whereas MA are predominantly located in the central & suprasellar region (20%) and associated with compression of the optic chiasm (7%). These findings align with prior MRI-based epidemiological studies, which demonstrate that microadenomas tend to be confined to one lobe due to their smaller size, while MA exhibit superior extension patterns and mass effect on surrounding structures. The high proportion of MA in the suprasellar region is clinically significant, given their strong correlation with visual pathway involvement and potential for delayed diagnosis . Additionally, the predominance of "normal scan" cases (25%) classified as non-adenomas highlights the importance of careful radiological-pathological correlation to avoid overdiagnosis in incidental findings .The statistical significance ($p < 0.001$) underscores a robust association between tumor type and anatomical distribution, emphasizing that tumor size and biological behavior are primary determinants of localization patterns, consistent with prior high-resolution MRI series [26, 28, 104].

Table (23): Comparative Analysis of Pituitary Tumor Types in Relation of Intrinsic Anatomical Location

Tumors Type	Location of the mass of the Pituitary adenomas	mean ± Std. Deviation	Std. Error	Number of cases	Percent	Cumulative	P-value
Microadenoma	Left anterior lobe	1.0 ± 0.0	0.00	30	30.0%	30.0%	
Macroadenomas	Central & suprasellar	2.0 ± 0.0	0.00	20	20.0%	50.0%	
Microadenoma	Central pituitary adenoma	1.0 ± 0.0	0.00	7	7.0%	57.0%	< 0.001**
Macroadenomas	Compression Chiasm effects	2.0 ± 0.28	0.83	11	11.0%	68.0%	
Microadenoma	Right anterior lobe	1.0 ±0.0	0.00	7	7.0%	75.0%	
Non-adenomas	Normal scan	3.0 ± 0.0		25	25.0%	100.0%	
Total		1.81± 0.81	0.08	100			
Overall Cases%				100 Cases			

Fig 19 illustrates the proportional distribution of pituitary tumor locations as detected by DCE-MRI, showing that MIA in the left anterior lobe was the most frequent (30%), followed by non-adenomas with normal scans (25%) and MA involving the central and suprasellar regions (20%). Less frequent sites included MIA in the central pituitary (11%) and right anterior lobe (7%), as well as MA with chiasmal compression (7%).

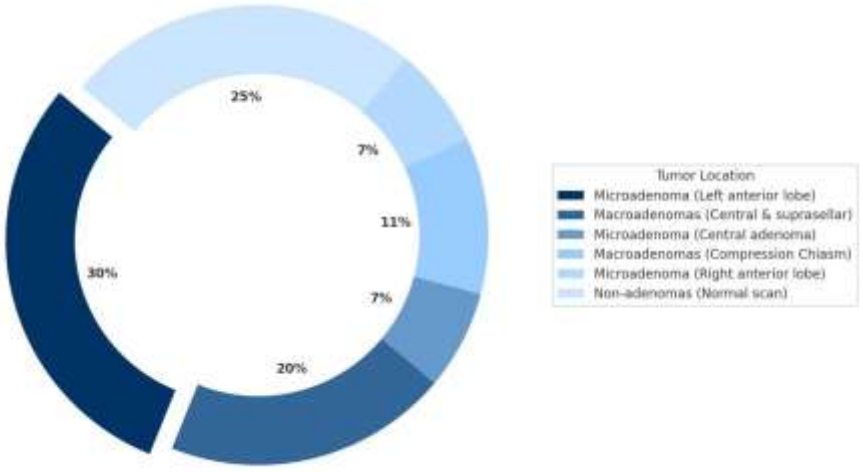

Fig (19): Exploded Donut Chart Illustrating the Distribution of Pituitary Tumor Locations Assessed by Dynamic Contrast- Enhanced (DCE) MRI.

Table 24 Headache was reported by 75% of the cohort, with the highest prevalence observed in MA with suprasellar extension and chasmal compression (≈82%) and in microadenomas extending suprasellar (≈85%). In contrast, the lowest proportion of headaches was observed in non-adenomatous lesions or normal MRI scans (60%). The association between headache and tumor type/location was statistically significant ($p < 0.001$.(This distribution is biologically plausible: larger lesions and those with suprasellar extension increase intrasellar pressure, stretch the diaphragma Sella, and compress the optic chasm and parasailer dura structures richly innervated by the trigeminal nerve, a well-known pathway for headache generation [55, 104, 105].

Table (24): Comparative Analysis of Pituitary Tumor Types by Anatomical Location and Headache Presence.

Tumor Type	Location of Tumor	Headache (Yes) n (%)	Headache (No) n (%)	Total n (%)	P-value
Microadenoma	Left anterior lobe	24 (80.0%)	6 (20.0%)	30 (30.0%)	
Microadenoma	Central pituitary adenoma	6 (85.7%)	1 (14.3%)	7 (7.0%)	<0.001**
Microadenoma	Right anterior lobe	5 (71.4%)	2 (28.6%)	7 (7.0%)	
Macroadenomas	Central & Suprasellar	16 (80.0%)	4 (20.0%)	20 (20.0%)	
Macroadenomas	Compression chiasm effects	9 (81.8%)	2 (18.2%)	11 (11.0%)	
Non-adenoma	Normal scan	15 (60.0%)	10 (40.0%)	25 (25.0%)	
Total		75 (75.0%)	25 (25.0%)	100 (100%)	

Fig 20 This figure illustrates the distribution of pituitary tumor locations and their association with headache prevalence. The largest segment corresponds to MIA located in the left anterior lobe (30%), followed by non-adenomatous lesions (25%) and macroadenomas involving the central and suprasellar regions (20%). Headaches were most frequently reported in patients with MA exhibiting suprasellar extension and chasmal compression (≈82%) and in microadenomas extending centrally (≈86%). In contrast, headache prevalence was lower in non-adenomatous lesions (60%) and microadenomas in the right anterior lobe (71%). These findings underscore the clinical significance of tumor location, as lesions compressing critical neurovascular structures are more likely to

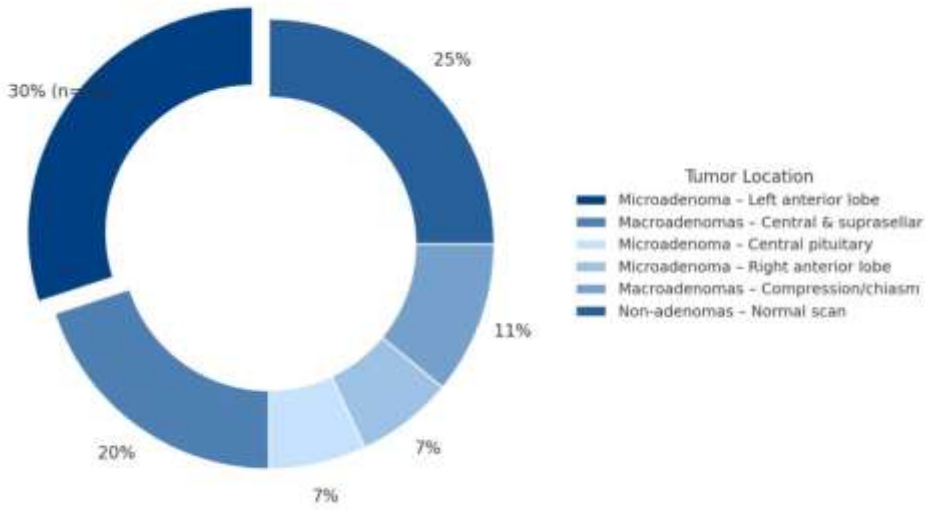

Fig (20): Exploded Donut Chart Depicting the Correlation Between Pituitary Tumor Location and Headache Presence.

Table 25 The results demonstrate a statistically significant difference ($p < 0.001$) among the groups. The highest prevalence of visual disturbances was observed in patients with macroadenomas located in the central and suprasellar region (90%) and those causing compression of the optic chiasm (90%). These findings are consistent with the well-known anatomical relationship between the suprasellar extension of macroadenomas and the proximity to the optic chiasm, which predisposes patients to visual field defects, particularly bitemporal hemianopia [106]. In contrast, no visual disturbances were reported in patients with microadenomas (0%), regardless of whether the lesion was in the left anterior lobe, right anterior lobe, or central pituitary region. This aligns with the fact that microadenomas (<10 mm) are generally confined to the Sella turcica and less likely to impinge on the optic apparatus [28]. Additionally, non-adenomatous lesions with normal imaging findings showed no visual disturbances in 100% of cases, further highlighting the correlation between tumor size, location, and the occurrence of visual symptoms.

Table (25): Comparative Analysis of Pituitary Tumor Types by Anatomical Location and Presence of Visual Disturbances.

Tumor Type	Location of Tumor	Visual Disturbance (Yes) n (%)	Visual Disturbance (No) n (%)	Number of Cases	Percent	Cumulative %	P-value
Microadenoma	Left anterior lobe	0 (0.0%)	30 (100%)	30	30.0%	30.0%	
Macroadenomas	Central & suprasellar	18 (90.0%)	2 (10.0%)	20	20.0%	50.0%	<0.001**
Microadenoma	Central pituitary adenoma	0 (0.0%)	7 (100%)	7	7.0%	57.0%	
Macroadenomas	Compression chiasm effects	10 (90.0%)	1 (9.1%)	11	11.0%	68.0%	
Microadenomas	Right anterior lobe	0 (0.0%)	7 (100%)	7	7.0%	75.0%	
Non-adenomas	Normal scan	0 (0.0%)	25 (100%)	25	25.0%	100.0%	
Total		28 (28.0%)	72 (72.0%)	100	100%	100%	

Fig 21 Macroadenomas with suprasellar extension demonstrated the highest proportion of visual symptoms (90%), reflecting their proximity to the optic chiasm and the high likelihood of chiasmal compression. In contrast, microadenomas in the left or right anterior lobe, and non-adenomatous lesions with normal MRI scans, showed no reported visual disturbances (0%), supporting existing evidence that small intrasellar lesions are less likely to impair visual pathways. Compression type MA also exhibited a high rate of visual symptoms (90%), further confirming that the extent and direction of tumor growth especially toward suprasellar and chiasmal regions are critical determinants of visual morbidity. This distribution aligns with previously reported patterns in which lesion size and anatomical extension are strong predictors of visual field defects, particularly bitemporal hemianopia, in Pituitary adenomas patients [47, 107].

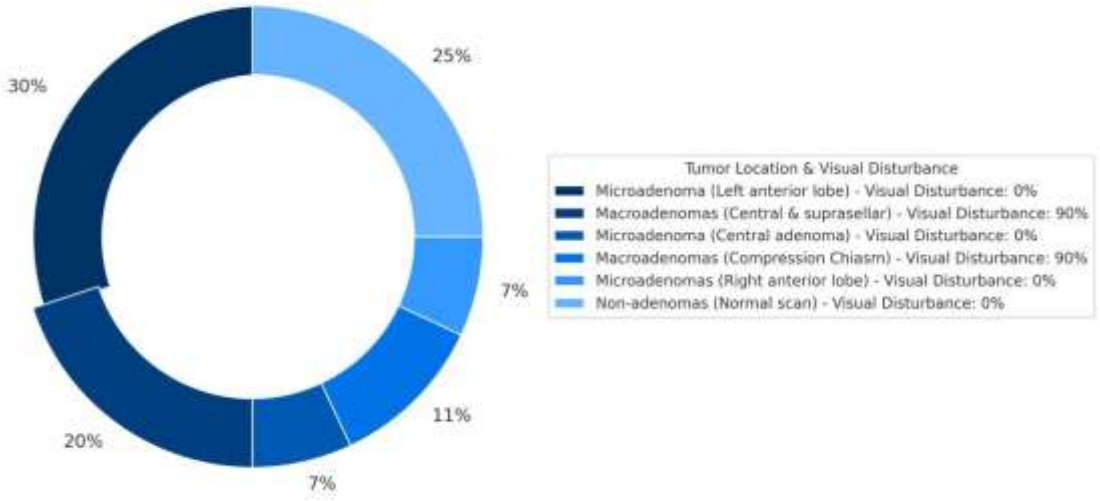

Fig (21): Exploded Donut Showing the Relationship Between Pituitary Tumor Location and the Presence of Visual Disturbances

Table 26 presents a confusion matrix comparing MRI diagnostic results with the prolactin reference standard for Pituitary adenomas. The matrix shows perfect agreement between MRI and the reference standard, with 75 true positives (MRI correctly identifying prolactin-positive adenomas) and 25 true negatives (MRI correctly

identifying prolactin-negative cases). There are no false positives or false negatives, indicating 100% sensitivity, 100% specificity, and 100% overall accuracy. Such results suggest that MRI, when interpreted alongside prolactin levels, is a highly reliable diagnostic tool for detecting Pituitary adenomas [31].

Table (26): Confusion Matrix Comparing MRI Diagnostic Results with Prolactin Reference Standard for Pituitary Adenomas

MRI vs. References Standard	Reference Positive	Reference Negative	Total
MRI Positive	75	0	75
MRI Negative	0	25	25
Total	75	25	100

Fig 22 demonstrates a perfect agreement between MRI findings and prolactin reference standards in diagnosing pituitary adenomas, with 100% sensitivity, specificity, positive predictive value (PPV), and negative predictive value (NPV). This indicates that MRI correctly identified all prolactin-positive adenomas (True Positives: 75 cases) and all normal cases (True Negatives: 25 cases) without any false positives or false negatives. Such accuracy aligns with previous literature reporting MRI as the gold standard imaging modality for pituitary adenomas, particularly dynamic contrast-enhanced MRI, which offers superior detection of microadenomas and assessment of tumor extension [31, 67].

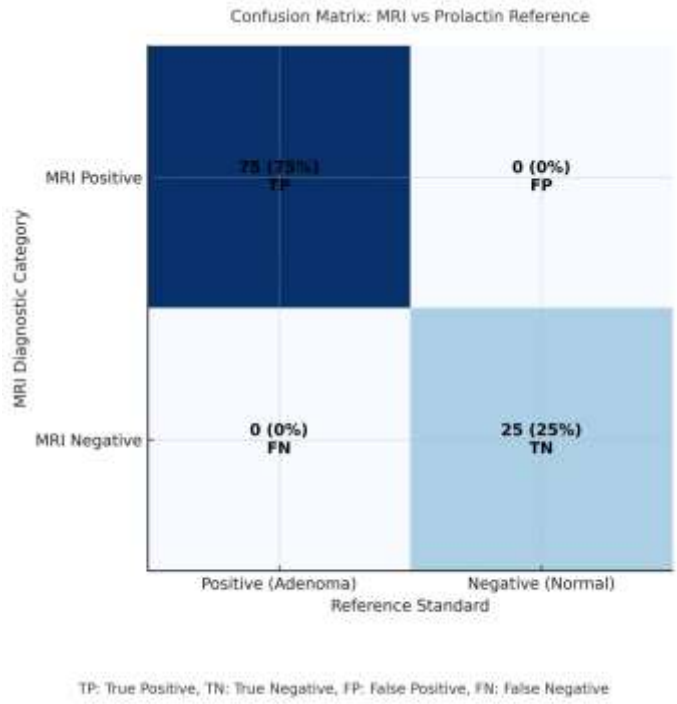

Fig (22): Confusion Matrix Comparing MRI Diagnostic Results with Prolactin Level as the References Standard for Pituitary Adenomas.

Table 26 demonstrates exceptional diagnostic performance of MRI in detecting pituitary adenomas when compared to prolactin levels as the reference standard, with 100% sensitivity, specificity, accuracy, positive predictive value (PPV), and negative predictive value (NPV). These findings indicate that MRI was able to correctly identify all true positive and true negative cases, with no false positives or false negatives, confirming its high reliability and diagnostic precision.Such perfect agreement is rarely observed in clinical practice and suggests that, in this cohort, MRI provided definitive confirmation of adenoma presence or absence without ambiguity. Comparable studies have also reported high diagnostic accuracy for MRI in pituitary adenomas, particularly when dynamic contrast-enhanced sequences are

utilized, as they allow for better delineation of tumor margins and detection of small lesions that may be missed on conventional imaging [31, 108, 109].

Table (26): Diagnostic Performance of MRI in Detecting Pituitary Adenomas Using Prolactin Levels as Reference Standard

Metric	Sensitivity	Specificity	Accuracy	Positive Predictive Value (PPV)	Negative Predictive Value (NPV)
Value (%)	100%	100%	100%	100%	100%

Fig 23 demonstrates the diagnostic performance of MRI in detecting Pituitary adenomas, with sensitivity, specificity, and accuracy all reaching 100%. This finding suggests that MRI, when correlated with prolactin levels, is highly reliable in differentiating pituitary adenomas from normal cases. Such perfect diagnostic values highlight MRI's central role as the imaging modality of choice for Sellar and parasailer lesions. Comparable studies have reinforced this high diagnostic performance. Emphasized the strong correlation between MRI features and pathological confirmation of pituitary adenomas, reporting near-perfect diagnostic indices in well-characterized cases. Similarly, reported MRI as the most sensitive imaging tool for pituitary lesions, particularly when combined with DCE-MRI sequences. However, while this figure indicates ideal values, it is important to note that in broader clinical practice, sensitivity and specificity may vary depending on tumor size, location, and radiologist expertise [28, 110, 111, 112].

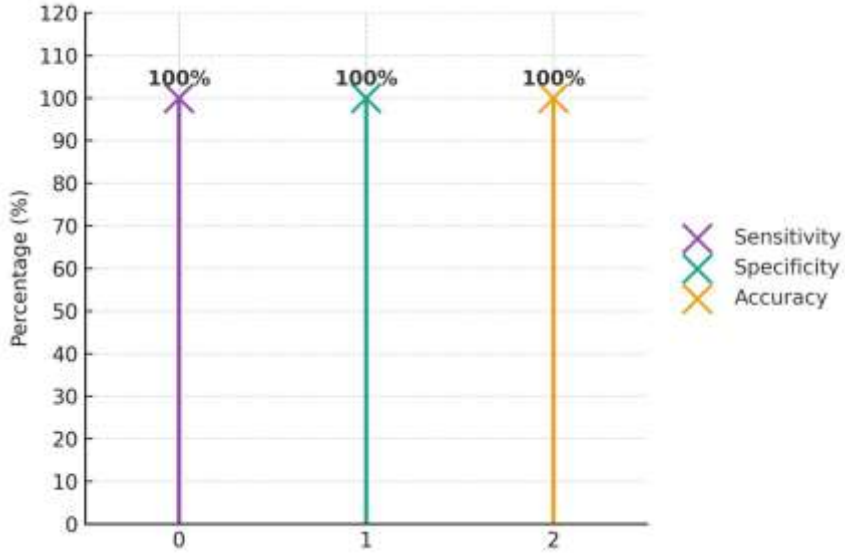

Fig (23): Lollipop Chart Illustrating the diagnostic performance of MRI in detecting pituitary adenomas, showing sensitivity, specificity, and accuracy values expressed as percentages

Fig.24 MRI appearance of pituitary microadenoma in a 26-year-old female patient with elevated serum prolactin, menstrual irregularity, galactorrhea, and persistent headache. A. 24 axial T2-WI TSE brain shows no obvious intracranial mass lesion and provides general brain assessment. B. 24 sagittal T2-WI pituitary demonstrates a small focal lesion within the anterior pituitary gland. C. 24 sagittal pre-contrast T1-WI SE shows a small hypointense lesion compared with the surrounding pituitary tissue. D. 24 coronal T2-WI TSE pituitary confirms a small lesion within the left side of the pituitary gland, measuring less than 10 mm. E. 24 coronal pre-contrast T1-WI shows a well-defined hypointense pituitary lesion without suprasellar extension. F. 24 coronal dynamic contrast-enhanced T1-WI demonstrates early relative hypo enhancement of the lesion compared with the normal enhancing gland. G. 24 sagittal delayed post-contrast T1-WI at 3 min shows subtle delayed enhancement of the lesion. H. 24 coronal delayed post-contrast T1-WI at 5 min confirms gradual enhancement while the lesion remains distinguishable from the surrounding gland.

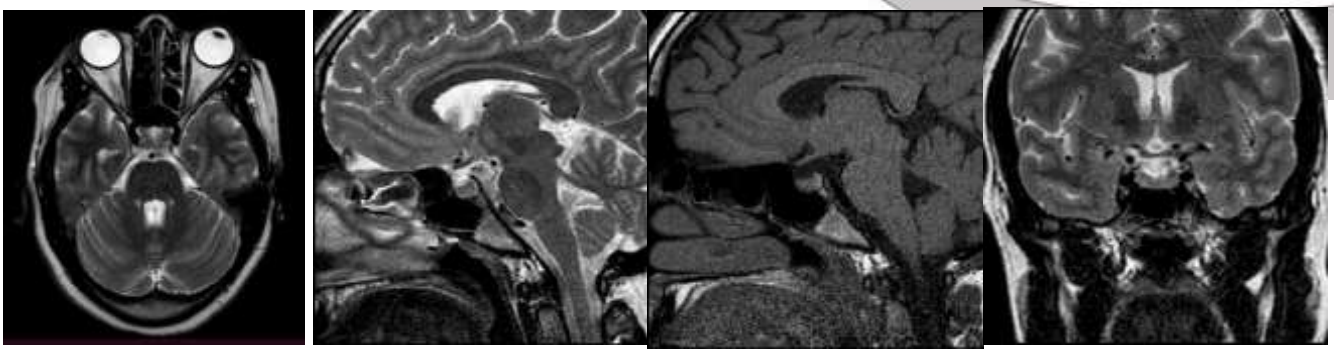

A-T2WI-TSE-axial brain. B-T2WI-TSE sagittal pituitary. C-T1WI-SE pre sagittal pituitary. D-T2W-TSE Coronal pituitary.

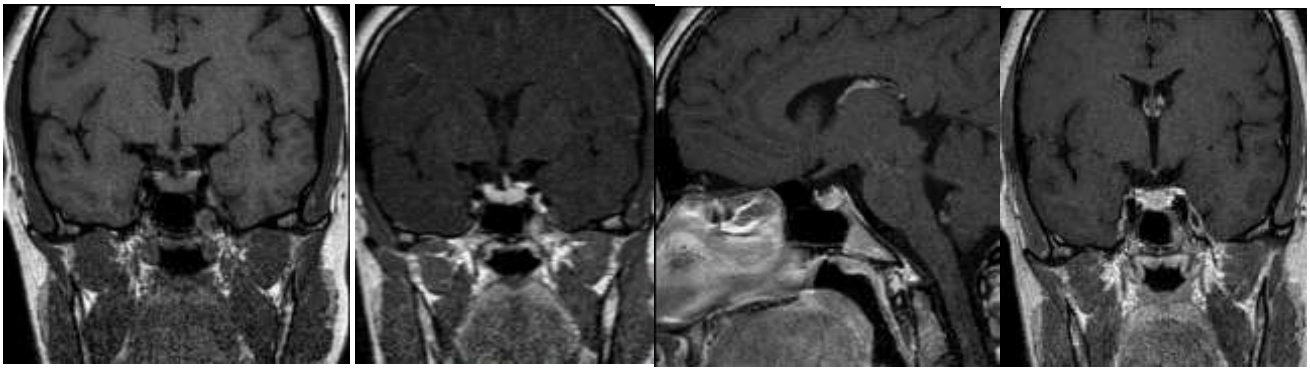

E-T1-WI-SE Coronal pre. F-T1+c Dynamic study coronal. G-T1+c sagittal delay Gd.3min. H- T1+c coronal delay Gd.5min

FIG 24. shows, integrating conventional MRI, dynamic contrast enhancement (DCE-MRI), delay post-contrast sequence in the context of Pituitary adenomas of a MIA for the pituitary protocols. A. T2WI-TSE-for the brain. B. T2WI-TSE Sagittal plane pituitary. C. T1WI-SE pre-contrast sagittal plane pituitary. D. T2W-TSE Coronal Pit. E. T1-WI-SE Coronal pre-contrast. F. T1-WI-dynamic study coronal plane during injection Gd. contrast agents. G. T1-WI sagittal plane, delay Gd.3min post-contrast injection. H. T1-WI coronal plane delay Gd.5min post-contrast agents' injection.

Fig. 25. shows, 47-year-old male patient. A.25 axial T2-WI TSE for brain Shows no obvious intra-axial brain abnormality. B. 25 sagittal T2-WI TSE for pituitary Shows a large sellar mass extending superiorly toward the suprasellar region. C.25 Sagittal pre-contrast T1-WI SE demonstrates a large pituitary mass replacing the normal gland. D. 25 coronal T2-WI pituitary confirms a large sellar mass with heterogeneous signal intensity. E. 25 coronal pre-contrast T1-WI SE shows a well-defined sellar mass measuring more than 10 mm. F. 25 coronal dynamic contrast-enhanced T1-WI shows heterogeneous enhancement of the lesion after Gd. injection. G. 25 sagittal delayed post-contrast T1-WI at 3 min shows persistent heterogeneous enhancement of the sellar lesion. H. 25 coronal delayed post-contrast T1-WI at 5 min confirms persistent heterogeneous enhancement with clear delineation of the pituitary macroadenoma.

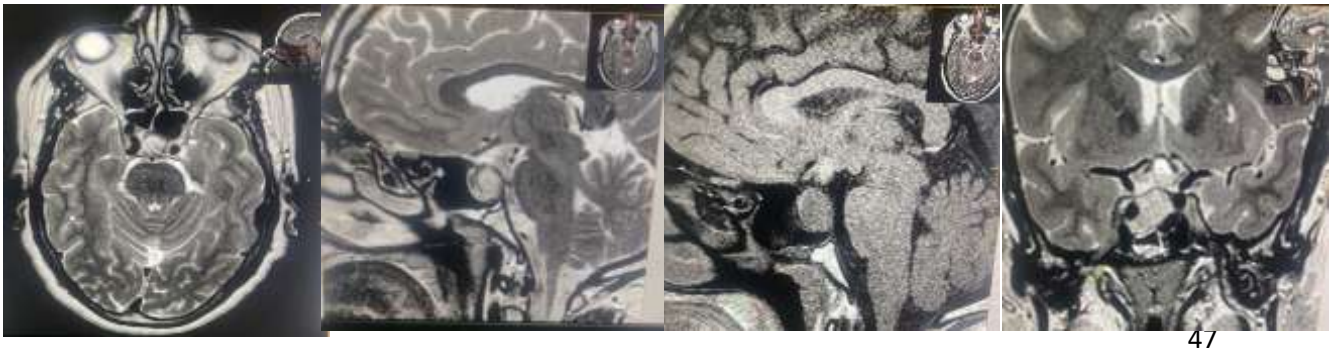

A-T2-WI-TSE axial Brain. B- T2-WI-TSE Sagittal Pit.G. C- T1-SE- pre-contrast sagittal Pit.G. D- T2-WI coronal Pit.G.

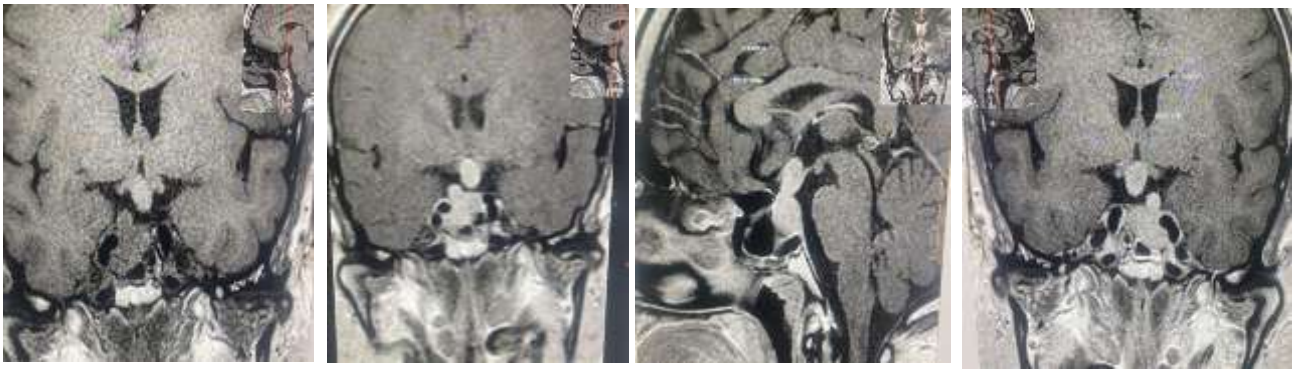

E-T1-WI-SE coronal pre. F- T1+c Dynamic study coronal. G-T1+c sagittal delay Gd.3min. H- T1+c coronal delay Gd.5min

FIG 25 shows pituitary macroadenomas. The mass appears as a large Sellar mass measuring more than 10mm, with Sellar expansion and suprasellar extension. A. T2WI-TSE-for the brain. B. T2WI-TSE Sagittal plane Pit.G. C. T1WI-SE pre-contrast sagittal plane Pit.G. D. T2W-TSE Coronal Pit. E. T1-WI-SE Coronal pre-contrast. F. T1-WI-dynamic study coronal plane during injection Gd. contrast agents. G. T1-WI SE sagittal plane, delay Gd.3min post-contrast injection. H. T1-WI SE coronal plane delay Gd.5min post-contrast agents' injection.

Conclusion:

1- MRI demonstrated high sensitivity for pituitary adenomas, with 75% of cases showing abnormal findings and significantly lower mean scores ($p < 0.001$).
2- Microadenomas are significantly more common in females, while macroadenomas are more prevalent in males, as supported by statistical significance ($p < 0.001$).
3- Macroadenomas present significantly later in life than microadenomas and non-adenomas, with a higher mean age ($p < 0.001$). These findings underline the importance of early screening in younger patients with microadenomas to prevent progression.
4- These results underline the importance of early detection of macroadenomas to prevent irreversible visual impairment. The consistent difference across groups demonstrates the utility of MRI and visual assessment in guiding timely surgical or medical intervention.
5- There was a significant association between prolactin levels and pituitary tumor type in males ($p < 0.001$). 72.2% of macroadenomas cases (13/18) showed severe prolactin elevation, while 100% of non-adenoma cases (8/8) had normal levels. These results highlight macroadenomas as the main cause of hyperprolactinemia in males, unlike non-functional tumors.
6- A clear gender-based difference was observed in prolactin patterns: females mostly had microadenomas with mild elevation (100%), while males predominantly showed macroadenomas with severe elevation (72.2%). Non-adenomatous tumors in both sexes showed normal prolactin levels (100%), confirming their non-functional nature. This highlights prolactin as a reliable marker for tumor type and stage across genders.
7- A statistically significant relationship was observed between menstrual pattern and pituitary tumor subtypes in females ($p< 0.001$). The majority of patients (58.9%) had irregular cycles, exclusively associated with microadenomas, while 23.3% with normal cycles were linked to non-adenomas. Amenorrhea (both primary and secondary) was found in 17.8% of cases, all due to macroadenomas, highlighting the clinical value of menstrual history in tumor differentiation.
8- Severe Galactorrhea was observed in 48.1% of male patients, indicating a strong link with macroprolactinomas and high prolactin levels. In contrast, 33.3% had no Galactorrhea, and 0% had moderate levels, revealing a clear bimodal clinical pattern useful for early tumor suspicion.

9- Galactorrhea was highly prevalent among female patients with pituitary tumors, with 58.9% exhibiting mild symptoms, indicating early-stage functional prolactinomas. In contrast, 10.8% showed severe Galactorrhea, likely reflecting larger macroadenomas, while 23.3% had no Galactorrhea, suggesting non-functional or non-adenomatous lesions. These findings highlight Galactorrhea as a reliable clinical marker that correlates with tumor functionality and prolactin activity in female patients.
10- the majority of microadenoma cases (58.9%) were associated with mild hyperprolactinemia and mild Galactorrhea, along with irregular menstrual cycles, suggesting early functional tumor activity. In contrast, macroadenomas demonstrated severe Galactorrhea (10.8%) and amenorrhea, reflecting advanced disease progression with high prolactin levels. Only 23.3% of female patients showed no Galactorrhea, likely indicating non-functional or non-adenomatous lesions, underscoring the strong correlation between tumor type, hormonal profile, and clinical manifestations.
11- Macroadenomas were the predominant tumor type among males with pituitary masses, with 48.1% of patients presenting severe Galactorrhea and elevated prolactin levels. In contrast, 29.6% of cases were non-adenomatous and hormonally silent.
12- Non-adenomatous lesions exhibited the highest T1 signal intensity (mean = 3.0, 29%) on pre-contrast MRI, followed by microadenomas with variable hypointense patterns (22%–12%), while macroadenomas consistently showed low signal intensity (mean = 1.0, 31%). These findings highlight a significant difference in pre-contrast T1-weighted imaging ($p < 0.001$), supporting its role in differentiating tumor subtypes based on tissue composition.
13- A significant variation in T2-WI MRI signal intensities across pituitary tumor types ($p < 0.001$), with macroadenomas (31%) presenting the lowest mean intensity (1.0) and non-adenomas (25%) exhibiting the highest (2.0). Microadenomas demonstrated intermediate and heterogeneous signal characteristics, particularly iso-hyperintense (22%) and iso–mild hyperintense (12%) patterns, underscoring the diagnostic value of T2 signal profiling in differentiating tumor subtypes.
14- Heterogeneous enhancing lesions represented the highest proportion (31%), followed by hypo-enhancing patterns (22%) and homogeneous early enhancing lesions (15%). Small delayed enhancing (12%) and focal delayed enhancing with contour distortion (10%) were less frequent but may indicate invasive or aggressive tumor behavior. The significant association ($p < 0.001$) highlights the value of dynamic contrast–enhanced (DCE-MRI) in differentiating pituitary tumor subtypes, particularly for identifying microadenomas and lesions with mass effect.
15- The analysis demonstrates that heterogeneous enhancement is the most prevalent dynamic contrast pattern, observed in 31% of cases, predominantly in macroadenomas. Hypoenhancement follows at 22%, mainly associated with microadenomas, while homogeneous enhancement accounts for 15% and reflects well-vascularized benign lesions. Both small delay enhancement and normal physiological enhancement are present in 12% and 10% of cases, respectively, with focal delay enhancement also at 10%, indicating localized fibrosis or vascular compromise.
16- Heterogeneous enhancement was the most prevalent DCE pattern (31.0%), most frequently observed in the left anterior lobe (31.0%) and central & suprasellar region (22.0%). Hypoenhancement was also common in these regions, indicating variable vascularity. These findings highlight a strong association between lesion location and enhancement pattern, which may reflect underlying tumor biology and aggressiveness.
17- Early heterogeneous enhancement (31.0%) and hypoenhancing lesions (22.0%) were most frequent, particularly among overweight and obese patients, suggesting a metabolic influence on tumor vascularity. These findings highlight the potential role of BMI in modulating pituitary adenoma imaging characteristics and guiding tailored diagnostic strategies.
18- microadenomas in the left anterior lobe were the most common finding (30%), followed by non-adenomas with normal scans (25%) and macroadenomas involving the central and suprasellar regions (20%). Less frequent locations included central pituitary microadenomas (11%), right anterior lobe microadenomas (7%), and macroadenomas with chiasmal compression (7%), highlighting a statistically significant distribution pattern ($p < 0.001$).
19- Headache is strongly associated with adenomatous lesions and suprasellar/chiasmal involvement, supporting the role of mass effect as the dominant mechanism. Tumor type and anatomical location should be considered in predicting headache burden and prioritizing management strategies.
20- Visual disturbance clustered almost exclusively in macroadenomas with suprasellar extension or chiasmal compression (90–91%, 28/31 macroadenomas sites), while it was absent in microadenomas

and non-adenomas (0%). This pattern indicates a strong association between chiasmal involvement and visual symptoms in pituitary disease (overall 28% vs. 72% without, $p < 0.001$).

21- A perfect agreement between MRI and the prolactin reference standard in diagnosing pituitary adenomas, with no recorded false positive or false negative cases. This indicates that both the sensitivity and specificity of MRI reached 100%, underscoring its reliability as a primary diagnostic tool for accurate and early detection in alignment with the reference standard.

22- The outstanding diagnostic performance of MRI in detecting pituitary adenomas, with sensitivity, specificity, and accuracy all reaching 100%. These findings highlight MRI's reliability as a gold standard tool when correlated with prolactin reference levels, confirming its capability to precisely differentiate adenomas from normal cases.

Limitation:

The study assessed headache only as a binary variable (yes, no) without stratification by severity or duration, which may limit detailed analysis of symptom burden among tumor subtypes. This study focused on qualitative assessment of dynamic enhancement patterns rather than quantitative pharmacokinetic modeling or time–intensity curve analysis. Although TIC could provide additional functional information, qualitative assessment remains clinically relevant and widely used in pituitary imaging.

References:

1- Zhai, J., Zheng, W., Zhang, O., Wu, J., Zhang, X. (2019), Pharmacokinetic analysis for the differentiation of pituitary microadenoma subtypes through dynamic contrast-enhanced magnetic resonance imaging. Vol. 17(%). PP: 4237-4244.

2- Jiang, X., Zhang, X. (2013), The Molecular Pathogenesis of Pituitary Adenomas: An Update. Endocrine and Material Journal. Vol.28, PP:245-254 http://creativecommons.org/licenses/by-nc/3.0/

3- Fernandez A, Karavitaki N, Wass J.A. (2010), Prevalence of pituitary adenomas: a community-based, cross-sectional study in Banbury (Oxfordshire, UK). Clin Endocrinol (Oxf), Vol.72, PP:377-82.

4- Ezzat S, Asa SL. (2006), Mechanisms of disease: the pathogenesis of pituitary tumors. Nat Clin Pract Endocrinol Metab. Vol.2, PP:220-30.

5- Buchfelder, M., Guaraldi, F., (2016), "Magnetic resonance imaging of pituitary tumors," Imaging Endocrine. Disorder., vol. 45, pp. 97–120.

6- Ganapathy, K. M., Tadi. P., (2023), Anatomy, Head and Neck, Pituitary Gland. in StatPearls [Internet], StatPearls Publishing.

7- Tsukamoto, T., Miki, Y., (2023). "Imaging of pituitary tumors: an update with the 5th WHO Classifications—part 1. Pituitary neuroendocrine tumor (Pit.NET)/pituitary adenoma," Jpn. J. Radiology., vol. 41(8), PP: 789–806,

8- Sadiq, M.N., Tadi, P., (2023) Physiology, Pituitary Hormones. StatPearls Publishing, Treasure Island (FL), Available: http://europepmc.org/abstract/MED/32491488

9- AL-Galabi, M., Bass, N. A., Alsalman, I., (2023), Physiology, Prolactin, StatPearls [Internet]. StatPearls Publishing; Treasure Island (FL).

10- Alyami, N., Alhenaki, G., Al Atwah, S., Alhenaki, N., Smaisem, F., Alotaibi, A. (2025), Correlation between MRI findings of pituitary gland and prolactin level among hyperprolactinemia adult female Saudi patients in rural areas. Observational study. Vol. 140(2). PP: 1-8.

11- Jhaveri, D.M., Salzman, L.K., Osborn, G.A. (2021), Anatomy Based diagnoses; sella and Pituitary. Fourth Edition. PP: 1143-1146.

12- Levy, B., Simon, A. J. (2024), A Contemporary view of menopausal hormone therapy. Clinical expert series. Vol. 144(1). PP: 12-23.

13- Tsukamoto, T., Miki, Y. (2023), Imaging of pituitary tumors: an update with the 5th WHO Classification-part 1. Pituitary neuroendocrine tumor (PitNET)/ pituitary adenoma. Japanese Journal of Radiology. Vol. 41(8). PP: 789-806.

14- H. S. (2022), Dynamic contrast-Enhanced MRI and its applications in various central nervous system diseases. IMRI Investigation Magnetic Resonance Imaging. Vol. 26(4). PP: 256-264.

15- Faul. F., Erdfelder, E., Buchner, A., Lang, A. G., (2009). Statistical power analyses using G-Power 3.1: Test for correlation and regression analyses. Behavior Research Methods. Vol41(4). PP:1149-1160. https://doi.org/10.3758/BRM.41.4.1149

16- Lakens, D. (2013). Calculating and reporting effect sizes to facilitate cumulative science: a practical primer for t-test and ANOVAs. Fortier's in Psychology. Vol.4. PP: https://doi.org/10.3389/fpsyg.2013.00863 .
17- Wu, Y., Li, D., Vermud, H.S. (2024), Advantages and Limitations of the Body Mass Index (IBM) to Assess Adult Obesity. International Journal of Environmental Research and Public Health. Vol. 21(757). PP:1-12.
18- A Healthy Lifestyle WHO Recommendations.(2010). Available online: https://www.who.int/europe/news-room/fact-sheets/item/a-healthy-lifestyle---who-recommendations
19- Melmed, S., Casanueva, F.F., Hoffman, R.A., Kleinberg, L.D., Montori, M.V., Schlechte, A.J., et al (2011), Diagnosis and Treatment of Hyperprolactinemia: An Endocrine Society Clinical Practice Guideline. The journal of clinical Endocrinology and Metabolism. Vol96(2). PP:273-288. https://doi.org/10.1210/jc.2010-1692
20- Mayo Clinic Laboratories, PROL-Prolactin, Serum https://www.mayocliniclabs.com/test-catalog/Overview/8402
21- Fitzgerald, P., Dinan, T.G. (2008), Prolactin and dopamine: what is the connection? Psychology of Journal. Vol22(2). PP: 12-19.
22- Halabia, L. S., Salih, Sh. A., (2005), Female hyperprolactinemia: analysis of presentation and diagnostic evaluation. Is pituitary Magnetic Resonance Imaging Always indicated?. Iraqi Journal of medical sciences. Vol. 4(1). PP:99-110.
23- Petersenn, S., Fleseriu, M., Casanueva, F. F., Giustina, A., Biermasz, M., Biller, K.M.B., (2023), Diagnosis and management of prolactin-secreting pituitary adenomas: a pituitary society international consensus statement. Nature Reviews Endocrinology. Vol. 19. PP:722-740
24- Melmed, S., Kaiser, B. U., Lopes, B. M., Bertherat, J., Syro, V. L., Ravert, G. et al (2022), Clinical Biology of the Pituitary Adenoma. Journal Clinical Endocrinol. Vol. 43. PP:1003-1037.
25- Colao, A., Savastano, S., (2011), Medical treatment of prolactinomas. Nature Reviews Endocrinology. Vol. 7(5). PP: 267-278.
26- Freda, U.P., Beckers, M.A., Katznelson, L., Molitch, E.M, Montor, M.V., Post, D.K., et al (2011), Pituitary Incidentaloma: An Endocrine Society Clini9cal Practice Guideline. Journal Clinical Endocrinol Metab. Vol. 96(4). PP:894-904.
27- Kassam, B.A., Prevedello, M.D., Snyderman, H.C., Thomas A., Gardner P., Zanation, A., et al (2008), Endoscopic endonasal skull base surgery: analysis of complications in the authors' initial 800 patients. Vol. 114(6). PP: 1344-1568.
28- Molitch, M.E. (2017), Diagnosis and treatment of pituitary adenomas: a review. Journal American Medical Association. Vol. 317(5). PP: 516-524.
29- Kumar, J.A., Leeds, E.N., Fuller, N,G., Tassel, V.P., Maor, H.M., Sawaya, E.R., Levin, A.V. (2000), Malignant Gliomas: MR Imaging Spectrum of Radiation Therapy-and Chemotherapy-induced Necrosis of the Brain after Treatment. Radiology Neuroradiology Journal. Vol. 217(2). PP: 539-551.
30- Lambru, G., Lagrata, S., Levy, A., Cheema, S., Davagnanam, I., Rantell, K. et al (2022)m Trigeminal microvascular decompression for short-lasting unilateral neuralgiform headache attacks. Vol. 145. PP: 2882-2893.
31- Rockall, A., Hatrick, A., Armstrong, P., Wastie, M. (213), Diagnostic Imaging. Seventh Edition. Wiley E-Text. PP:1-522
32- Westbrook, C., Roth, C.K., Talbot, J. (2022), MRI in Practice. Fifth Edition. Wiley-Blackwell. PP: 1-370
33- Reddy M.J.J. (2005), Step by step MRI. First Edition. Taylor & Francis New Delhi, PP: 1-299
34- Runge, M.V., Heverhagen, T.J. (2022), The Physics of Clinical MR Taught Through images. Fifth Edition. PP: 1-377
35- Liney, G., (2010), MRI from A to Z A Definitive Guide for Medical Professionals. Second Edition. Springer Dordrecht Heidelberg London New York. PP: 1-392.
36- Westbrook, C., Talbot, J. (2019), MRI in Practice. Fifth Edition. Wiley Blackwell. PP: 1-418
37- Kanel, E., Barkovich, A.J., Bell, C., et al (2021), ACR Manual on Contrast Media. American College of Radiology.
38- Tsukamoto, T., Miki, Y. (2023), Imaging of Pituitary Tumors: an update with the 5th WHO Classifications part2, Neoplasms other than PitNET and tumor mimicking lesions. Japanese Journal of Radiology. Vol. 41. PP: 808-829 https://doi.org/10.1007/s11604-023-01407-0
39- Westbrook, C. (2014), Handbook of MRI Technique. Fourth Edition. Cambridge, UK. PP:1-394.

40- Groves, M.E., Bireley, W., Dill, K., Carroll, J.T., Carr, C.J. (2007),Quantitative analysis of ECG-gated high-resolution contrast- enhanced MR Angiography of the thoracic aorta. American Roentgen Ray Society. Vol. 188(2). PP: 522-528
41- Bright, Anne. (2011), Planning and Positioning in MRI. First Edition. PP: 1-270.
42- AL-Qurayshi, R. M., AL-Mosawi, Q. H. (2015), Radiation Physics and its applications in diagnostic radiological techniques. First Edition. Baghdad, Iraq. PP: 1-303.
43- Pallant, J. (2020), SPSS Survival Manual A step by step guide to data analysis using IBM. Seventh Edition. PP:1-10
44- Sheskin, J. D. (20000, Handbook of Parametric and Nonparametric statistical procedures. Second Edition. PP: 1-972
45- Dorey, F. (2011). Statistics in brief: interpretation and use of p values: all p values are not equal. Clinical Orthopedics and Related Research®, 469(11), 3259-3261. DOI: 10.1007/s11999-011-2053-3
46- Akobeng, K.A. (2006). Understanding diagnostic tests1: sensitivity, specificity, and predictive values. Vol. 96 (3). PP: 338-341. https://share.google/lfINNvW6NI7TYHfaX
47- Altman, D. G. Bland J. M. (1994) Diagnostic tests 1: sensitivity and specificity. The BMJ. Vol. 308 (6943). PP: 1552.
48- Bossuyt, M. P., Reitsma, B. J., Bruns, E. D., Gatsonis A. C., Glasziou, P. P., Irwig, L. et al (2015), Stard 2015: An Updated List of Essential Items for Reporting Diagnostic Accuracy Studies. Vol. 277(3). PP: 351. https://doi.org/10.1148/radiol.2015151516
49- Verhelst, J., Abs, R., Maiter, D., et al (1999), Cabergoline in the treatment of hyperprolactinemia: a study in 455 patient. Journal Clinical Endocrinol Metab. Vol. 84(7). PP: 2518-2522.
50- Shimon, I., Sosa, E., Mendoza, V., Greenman, Y., Tirosh, A., Espinosa, E. (2016), Giant prolactinomas larger than 60 mm in size: a cohort of massive and aggressive prolactin-secreting pituitary adenomas.
51- Colao, A., Sarno, D.A., Cappabianca, P., Somma, D.C., Pivonello, R., Lombardi, G. (2003), Withdrawal of long-Term Cabergoline Therapy for Tumoral and Nontumoral Hyperprolactinemia. The New England Journal of Medicine. Vol. 349(21). PP: 2023- 2033.
52- Greenman, Y., Limor, R., Yaron, M., Sterm, N. (2004), Ghrelin secretion is modulated in a nutrient-and gender-specific manner. Journal Clinical Endocrinology. Vol. 60. PP: 382-388.
https://www.researchgate.net/publication/5589204
53- Ho, y. k. k., Kaiser, B. U., Melmed, S. (2023), Pituitary adenoma or neuroendocrine tumor: the need for an integrated prognostic classification. Nature Reviews endocrinology. Vol. 19. PP: 671-678.
54- Manov, E.A., et al (2024), Pituitary Microadenomas. Medicine Endocrinology Medscape.
55- Bonneville, F.J. (2024), Tricks and Traps in MRI of the Pituitary Region. Springer Nature Switzerland AG. PP:1-246
56- Prezioso, G., Giannini, C., Chiarelli, F. (2028), Effect of Thyroid Hormones on Neurons and Neurodevelopment. Hormones Research in Pediatrics. Vol. 90(2). PP: 73-81.
https://doi.org/10.1159/000492129
57- Ezzat, S., Asa, L. S., Couldwell, T. W., Barr, E. C., Dodge, E. W., Vance, L. M. (2004), The Prevalence of Pituitary Adenomas. American Cancer Society. Vol. 101(3). PP: 613-619.
58- Kou, I., Saisho, Y., Sato, S., Yamada, T., Itoh, H. (2014), Islet Number Rather Than Islet Size Is a Major Determinant of B-and a-Cell Mass in Humans. Journal of Clinical Endocrinology & Metabolism. Vol. 99(5). PP: 1733-1740.
59- Dekkers, M.O., Pereira, M.A., Romijn, A.J. (2008), Treatment and Follow-Up of Clinically Nonfunctioning Pituitary Macroadenomas. The Journal of Clinical Endocrinology& Metabolism, Vol. 93(10). PP: 3717-3726.
https://doi.org/10.1210/jc.2008-0643
60- Cooney, M. J., Lucey, V. J., Dinan, G. T. (2018), Enhanced growth hormone responses to pyridostigmine challenge in patients with panic disordered. The British Journal of Psychiatry. Vol. 170(2). PP: 159-161.
61- Raverot, G., Burman, P., MuCormack, A., Heaney, A., Petersenn, S., Popovic, V. (2018), European Society of Endocrinology Clinical Practice Guidelines for the management of Aggressive pituitary tumors and carcinomas. The European Journal Society of Endocrinology. Vol. 178. PP: 1-24
62- Freda, P., Beckers, M. A., Katznelson, L., Molitch, M., Montori, M. V., Post, D. K. et al (2011), Pituitary Incidentaloma: An Endocrine Society Clinical Practice Guideline. Journal Clinical Endocrinol Metab. Vol. 96(4). PP: 894-904.

63- Fleseriu, M., Christ-Crain, M., Langlois F., Gadelha, M., Melmed, S. (2024), Hypopituitarism. The Lancet. Vol. 403(10444). PP: 2632-2648.
64- Yavropoulou, P. M., Tsoli, M., Barkas. K., Kaltsas, G., Grossman, A. (2020), Journal Endocrine-Related Cancer. Vol. 27. PP: 375-390. https://erc.bioscientifica.com https://doi.org/10.1530/ERC-20-0136
65- Tagoe, N. N., Essuman, A. V., Bankah, P., Dakurash, T., Hewlett, K. V., Akpalu, J. et al (2019) Ethiopian Journal of Health Science. Vol. 29(1). PP: 895-902.
66- Melmed. S., Casanueva, F. F., Cavagnini, F., Chanson, P., Frohman, L., Grossman, A., et al (2002), Guidelines for Acromegaly Management. Vol. 87(9). PP: 4054-4058.
67- (2016), Congress of neurological surgeons systematic review and evidence-based guideline on posttreatment follow-up evaluation of patients with nonfunctioning pituitary adenomas. Vol. PP: 1- 54.
68- Verhelst, J., Abs, R, (2009), Cardiovascular risk factors in hypopituitary GH-deficient adults. European Journal of Endocrinology. Vol. 161. PP: 41-40.
69- Cooper, O., Greenman, Y. (2018), Dopamine agonists for pituitary adenomas, Frontiers in endocrinology. Vol. 9. PP: 469.
70- Bendarska-Czerwinska, A., Zmarzty, N., Morawiec, E., Panfil, A., Brys, K., Czarniecka, J. (2023), Endocrine disorders and fertility and pregnancy: An update. Journal Frontiers in Endocrinology. Vol. 17. PP: 1-30.
71- Bonnevile, F. J., Potorac, I., Petrossians, P., Tshibanda, L., Beckers, A. (2022), Pituitary MRI in Cushing's disease – an update. Journal of Neuroendocrinology. Vol. 34(8), PP: 13115
72- Mancini, A., Vergani, E., Bruno, C., Glaudia, G., Spaziani, M., Isidori, M. A. et al (2023), Vol. 14.
73- Islam, S, Afrin, S., Jones, I. S., Segars, J. (2020), Selective Progesterone Receptor Modulators Mechanisms and Therapeutic Utility. Journal Endocrine Reviews. Vol. 41(5). PP: 1-52.
74- Akirov, A., Asa, L. S., Larouche, V., Mete, O., Sawka, M. A., Jang, R. (2019), The Clinicopathological Spectrum of Parathyroid Carcinoma. The Journal Cancer Endocrinology. Vol. 10. PP: 731.
75- Fukuhara, N., Nishiyama, M., Lwasaki, Y. (2022), Update, in Pathogenesis, Diagnosis, and Therapy of Prolactinomas. The Journal of Cancer. Vol. 14(15). PP: 1-13.
76- Aziz, K., Shahbaz, A., Umair, M., Sharifzadeh, M., Sachmechi, I. (2018), Hyperprolactinemia with Galactorrhea due to subclinical and review of literature. National Library of Medicine NIH Journal. Vol. 10(5). PP: 1-5.
77- Mahmoud, M. M., Haj-Ahmad, M. L., Sweis, G. W. N., Nsour, A. O., Al-Ani, T. A., Oran, O. et al (2025), Clinical Features and Hormonal Profile of Macroprolactinomas Presenting With the Hook Effect: A Systematic Review. The Journal Endocrine Practice. Vol. 31(2). PP: 215-225.
78- Fnu, Y., Sameer Abdul, R., Muskan, D., Komal, I., Rubayyi, A., Prashant, K. A. (2024), Prolactinoma: Navigating the Dual Challenge of side Effects and Treatment Strategies- A Comprehensive Review. The Journal Analysis of Medicine & Surgery. Vol. 86(8). PP: 4613-4623.
79- Haidenberg-Davis, T. J., Cedars, M. I., Rebar, R. W., ACOG Committee on Practice Bulletins-Gynecology. (2024). Current evaluation of amenorrhea: a committee opinion. American Society for Reproductive Medicine ASRM. Vol. 122(1). PP: 52-61.
80- Benetti-Pinto, C. L., Nacul, A. P., Rosa e Silva, A. C., Nogueira, V. S., Elias, P. C., et al (2024), Hyperprolactinemia in women: treatment. Febrasgo Position statement. Vol. 5. PP: 1- 10.
81- Iglesias, P., Diez, J. J. (2013), Macroprolactinoma: a diagnostic and therapeutic update. An International Journal of Medicine. Vol.106(6). PP: 495-504.
82- Bonneville, J. F., Bonneville, F., Cattin, F. (2005), Magnetic resonance imaging of pituitary adenomas. European radiology. Vol. 15(3). PP: 543-548.
83- Xekouki, P., Lodge, J. E., Matschke, J., Santambrogio, A., Apps, R. J., Sharif, A. et al (2019), Non-secreting pituitary tumors characterized by enhanced expression of YAP/TAZ. Frontiers in Endocrinology. Vol. 10. PP: 816.
84- Tsukamoto, T., Miki, Y. (2023), Imaging of pituitary tumors: an update with the 5th WHO Classifications part 1. Pituitary neuroendocrine tumor (PitNET)/pituitary adenoma. Japanese Journal of Radiology. Vol. 41. PP: 789-806.
85- Agosti, E., Cuocolo, R., Mangili, M., Rampinelli, V., Veiceschi, P. et al (2025), Radiomics for Preoperative Assessment of Pituitary Adenoma Consistency with T2-Weigjhted MRI: A Multicenter Study.
86- Hwang, K., Bae, J. Y., Kim, C., Lee, H. D., Jeong, Y. S., Cho, J. S. (2025), Comparison of gadobutrol and meglumine gadoterate for dynamic contrast-enhanced MRI of pituitary macroadenomas. Scientific reports. Vol. 15. PP: 1-11.

87- Shih, Y. R., Schroeder, W. J., Koeller, K. K. (2021), Primary Tumors of the Pituitary Gland: Radiologic-Pathologic Correlation. Radio Graphics Journal. Vol. 41. PP: 2029-2046.
88- Liu, Z., Hou, B., You, H., Lu, L., Duan, L., Li, M. et al (2023), High-resolution contrast-enhanced MRI with three-dimensional fast spin echo improved the diagnostic performance for identifying pituitary microadenomas in Cushing's syndrome. National Library of Medicine NIH Journal. Vol. 33(9). PP: 5984-5992.
89- Miki, Y., Matsuo, M., Nishizawa, S., Kuroda, Y., Keyaki, A., Makita, Y. (1990), Pituitary adenomas and normal pituitary tissue: enhancement patterns on gadopentetate-enhanced MR Imaging. Radiology Journal. Vol. 177(1), PP:
90- Osawa, I., Nagawa, K., Hara, Y., Shimizu, H., Tanaka, S., Kozawa, E. (2023), Utility of contrast-enhanced 3D STIR FLAIR imaging for evaluating pituitary adenomas at 3 Tesla. European Journal of Radiology Open. Vol. 11(100500). PP: 1-8.
91- Bonneville, J.F., Potorac, J., Beckers, A. (2020), Neuroimaging of aggressive pituitary tumors. Endocrine and Metabolic Disorders Journal. Vol. 21(2), PP: 235-242.
92- Hagiwara, A., Inoue, Y., Wakasa, K., Haba, T., Tashiro, T., Miyamoto, T. (2003), Comparison of growth hormone-producing and non-growth hormone-producing pituitary adenomas: imaging characteristics and pathologic correlation. RSNA Radiology. Vol. 22892). PP: 533-538.
93- Zada, G., Woodmansee, W. W., Ramkissoon, S., Amadio, J., Nose, V., Laws, R.E. (2011), Atypical pituitary adenomas: incidence, clinical characteristics, and implications. Journal of neurosurgery. Vol. 114(2), PP: 336-344.
94- Hwang, M. J., Kim, H. Y., Kim, W. J., Kim, G. D., Jung, W. H., Chung, S.Y. (2013), Feasibility of endoscopic endonasal approach for recurrent pituitary adenomas after microscopic trans-spheroidal approach. Journal of Korean Neurosurgical Society. Vol. 54(4). PP: 317-322.
95- Kucharczyk, W., Bishop, E. J., Plewes, B. D., Keller, A. M., George, S. (1994), Detection of pituitary microadenomas; comparison of dynamic keyhole fast spin-echo, unenhanced, and conventional contrast-enhanced MR imaging. American journal of roentgenology AJR. Vol. 163(3). PP: 671-679.
96- Lucas. W. J., Zada, G., (2012), Imaging of the pituitary and Parasellar Region. Semin Neural. Vol. 32(04). PP: 320-331.
97- Bartynski, S. W., Lin, L. (1997), Dynamic and Conventional Spin-Echo MR of Pituitary Microlesions. AJNR American Journal Neuroradial. Vol. 18. PP: 965-972.
98- Yuh, C. T. W., Fisher, J. D., Nguyen, D. H., Tali, T. E., Gao, F., Simonson, M. T., Schlechte, A. J. (1994), Sequential MR Enhancement Pattern in Normal Pituitary Gland and in Pituitary Adenoma. AJNR American Journal Neuroradial. Vol. 15. PP: 101-108.
99- Kanou, Y., Arita, K., Kurisu, K., Tomohide, A., Lida, K., (2002), Clinical implications of dynamic MRI for pituitary adenomas: clinical and histologic analysis. Vol. 9(6). PP: 659-663.
100- Sen, R., Sen, C., Pack, J., Block, T. K., Golfinos, G. J., Prabhu, V. (2017), Role of high-resolution dynamic contrast-Enhanced MRI with Golden-Angle Radial Sparse Parallel Reconstruction to Identify the Normal Pituitary Gland in Patients with Macroadenomas. AJNR American Journal Neuroradial. Vol. 38(6). PP: 1117-1121.
101- Baert, L. A., Heuck, W. H. F., Youker, E. J. (2012), Radiology Imaging of Endocrine Disease. Springer Science & Business Media.
102- Jalilianhasanpour, R., Ryan, D., Agarwal, S., Gujar, S., Pillai, J., Sair, H. et al Dynamic Brain Connectivity in Resting State Functional MR Imaging. Neuroimaging Clinics. Vol. 31(1). PP: 1-92.
103- Zoli, M., Guaraldi, F., Faustini, M., Mazzatenta, D. (2018), Myasthenia gravis imitating pituitary apoplexy in macroprolactinoma. International Journal of Endocrinology and Metabolism. Vol. 17. PP: 423-426.
104- Schankin, J. C., Reifferscheid, K. A., Krumbholz, M., Linn, J., Rachinger, W., Sostak, P. et al (2012), Headache in patients with pituitary adenoma: Clinical and parclinical findings. International Headache Society SAGE Journal. Vol. 32(16). PP: 1198-1207.
https://journals.sagepub.com/doi/epub/10.1177/0333102412462639
105- Levaru, J. M., Matharu, S.M., Meeran, K., Powell, M., Goadsby, J. P., (2005), The clinical characteristics of headache in patients with pituitary tumors. Journals.permissions@oupjournals.org. Vol. 128(8). PP: 1921-1930. https://doi.org/10.1093/brain/awh525
106- Norden, D. A., Reardon, A. D., Wen, C. Y. P. (2011), Primary Central Nervous System Tumors. First Edition. PP: 1-570

107- Chowdhury, S., Hasan, M., Rahman, M. A., Ahmed, M. F., Islam, K. A., Ratul, R. H. (2023), Clinical, hormonal, and radiological characteristics of patients with sellar mass at a neurosurgical unit of a neuro-specialized hospital in Dhaka.
108- Journal of Association of Clinical Endocrinologist and Dialectologist of Bangladesh, Vol. 2(1), PP: 14-18.
109- Amin, R., Nath, D. H., Hossain, M., Barua, K. K., (2012), Early Post-operative Visual Outcome in Patient with Pituitary Adenoma. Bangladesh Journal of Neuroscience. Vol. 28(2). PP: 108-115.
110- Lithgow, K., Batra, R., Matthews, T., Karavitaki, N. (2019), Management of endocrine disease: visual morbidity in patients with pituitary adenoma. European Journal of Endocrinology, Vol. 181(5). PP: 185-197.
111- Salehi, F., Kovacs, K., Scheithauer, W. B., Lloyd, V. R., Cusimano, M. (2006), Pituitary tumor-transforming gene in endocrine and other neoplasms: a review and update. Endocrine-Related Cancer. Vol. 15. PP: 721-743.
112- Leca, M. B., Mytilinaiou, M., Tsoli, M., Epure, A., Aylwin, B. J. S., Kaltsas, G. (2021), Identification of an optimal prolactin threshold to determine Prolactinoma size using receiver operating characteristic analysis. Scientific reports. Vol. 11(1). report 9801. PP: 1-7